4. Igarashi Y, Tamura Y, Suzuki K, Tanabe Y, Yamaguchi T, Fujita T, Yamazoe M, Aizawa Y, Shibata A. Coronary artery spasm is a major cause of sudden cardiac arrest in survivors without underlying heart disease. *Coron Artery Dis.* 1993;4:177–185.
5. Miller DD, Waters DD, Szlachcic J, Theroux P. Clinical characteristics associated with sudden death in patients with variant angina. *Circulation.* 1982;66:588–592.
6. Campos E, Nakajima K, Tanaka A, Havel RJ. Properties of an apolipoprotein E-enriched fraction of triglyceride-rich lipoproteins isolated from human blood plasma with a monoclonal antibody to apolipoprotein B-100. *J Lipid Res.* 1992;33:369–380.
7. Nakajima K, Saito T, Tamura A, Suzuki M, Nakano T, Adachi M, Tanaka A, Tada N, Nakamura H, Campos E, Havel RJ. Cholesterol in remnant-like lipoproteins in human serum using monoclonal anti apo B-100 and anti apo A-I immunoaffinity mixed gels. *Clin Chim Acta.* 1993;223:53–71.
8. McNamara JR, Shah PK, Nakajima K, Cupples LA, Wilson PW, Ordovas JM, Schaefer EJ. Remnant-like particle (RLP) cholesterol is an independent cardiovascular disease risk factor in women: results from the Framingham Heart Study. *Atherosclerosis.* 2001;154:229–236.
9. Kugiyama K, Doi H, Takazoe K, Kawano H, Soejima H, Mizuno Y, Tsunoda R, Sakamoto T, Nakano T, Nakajima K, Ogawa H, Sugiyama S, Yoshimura M, Yasue H. Remnant lipoprotein levels in fasting serum predict coronary events in patients with coronary artery disease. *Circulation.* 1999;99:2858–2860.
10. Takeichi S, Yukawa N, Nakajima Y, Osawa M, Saito T, Seto Y, Nakano T, Saniabadi AR, Adachi M, Wang T, Nakajima K. Association of plasma triglyceride-rich lipoprotein remnants with coronary atherosclerosis in cases of sudden cardiac death. *Atherosclerosis.* 1999;142:309–315.
11. Sakata K, Miho N, Shirotani M, Yoshida H, Takada Y, Takada A. Remnant-like particle cholesterol is a major risk factor for myocardial infarction in vasospastic angina with nearly normal coronary artery. *Atherosclerosis.* 1998;136:225–231.
12. Shimokawa H. Rho-kinase as a novel therapeutic target in treatment of cardiovascular diseases. *J Cardiovasc Pharmacol.* 2002;39:319–327.
13. Shimokawa H. Cellular and molecular mechanisms of coronary artery spasm: lessons from animal models. *Jpn Circ J.* 2000;64:1–12.
14. Shimokawa H, Ito A, Fukumoto Y, Kadokami T, Nakaike R, Sakata M, Takayanagi T, Egashira K, Takeshita A. Chronic treatment with interleukin-1 beta induces coronary intimal lesions and vasospastic responses in pigs in vivo. The role of platelet-derived growth factor. *J Clin Invest.* 1996;97:769–776.
15. Kandabashi T, Shimokawa H, Miyata K, Kunihiro I, Kawano Y, Fukata Y, Higo T, Egashira K, Takahashi S, Kaibuchi K, Takeshita A. Inhibition of myosin phosphatase by upregulated rho-kinase plays a key role for coronary artery spasm in a porcine model with interleukin-1beta. *Circulation.* 2000;101:1319–1323.
16. Morishige K, Shimokawa H, Eto Y, Kandabashi T, Miyata K, Matsumoto Y, Hoshijima M, Kaibuchi K, Takeshita A. Adenovirus-mediated transfer of dominant-negative rho-kinase induces a regression of coronary arteriosclerosis in pigs in vivo. *Arterioscler Thromb Vasc Biol.* 2001;21:548–554.
17. Masumoto A, Mohri M, Shimokawa H, Urakami L, Usui M, Takeshita A. Suppression of coronary artery spasm by the Rho-kinase inhibitor fasudil in patients with vasospastic angina. *Circulation.* 2002;105:1545–1547.
18. Ohara N, Takeichi S, Naito Y, Nakajima Y, Yukawa N, Nakano T, Nakajima K. Remnant-like particles from subjects who died of coronary artery disease suppress NO synthase activity and attenuate endothelium-dependent vasorelaxation. *Clin Chim Acta.* 2003;338:151–156.
19. Oshiro N, Fukata Y, Kaibuchi K. Phosphorylation of moesin by rho-associated kinase (Rho-kinase) plays a crucial role in the formation of microvilli-like structures. *J Biol Chem.* 1998;273:34663–34666.
20. Fukata Y, Kimura K, Oshiro N, Saya H, Matsuura Y, Kaibuchi K. Association of the myosin-binding subunit of myosin phosphatase and moesin: dual regulation of moesin phosphorylation by Rho-associated kinase and myosin phosphatase. *J Cell Biol.* 1998;141:409–418.
21. Ichiki T, Usui M, Kato M, Funakoshi Y, Ito K, Egashira K, Takeshita A. Downregulation of angiotensin II type 1 receptor gene transcription by nitric oxide. *Hypertension.* 1998;31:342–348.
22. Kugiyama K, Doi H, Motoyama T, Soejima H, Misumi K, Kawano H, Nakagawa O, Yoshimura M, Ogawa H, Matsumura T, Sugiyama S, Nakano T, Nakajima K, Yasue H. Association of remnant lipoprotein levels with impairment of endothelium-dependent vasomotor function in human coronary arteries. *Circulation.* 1998;97:2519–2526.
23. Kawakami A, Tanaka A, Nakajima K, Shimokado K, Yoshida M. Atorvastatin attenuates remnant lipoprotein-induced monocyte adhesion to vascular endothelium under flow conditions. *Circ Res.* 2002;91:263–271.
24. Kawakami A, Tanaka A, Chiba T, Nakajima K, Shimokado K, Yoshida M. Remnant lipoprotein-induced smooth muscle cell proliferation involves epidermal growth factor receptor transactivation. *Circulation.* 2003;108:2679–2688.
25. Twickler TB, Dallinga-Thie GM, Visseren FL, de Vries WR, Erkelens DW, Koppeschaar HP. Induction of postprandial inflammatory response in adult onset growth hormone deficiency is related to plasma remnant-like particle-cholesterol concentration. *J Clin Endocrinol Metab.* 2003;88:1228–1233.
26. Cohn JS, Marcoux C, Davignon J. Detection, quantification, and characterization of potentially atherogenic triglyceride-rich remnant lipoproteins. *Arterioscler Thromb Vasc Biol.* 1999;19:2474–2486.
27. Karpe F. Postprandial lipoprotein metabolism and atherosclerosis. *J Intern Med.* 1999;246:341–355.
28. Bjorkegren J, Silveira A, Boquist S, Tang R, Karpe F, Bond MG, de Faire U, Hamsten A. Postprandial enrichment of remnant lipoproteins with apoC-I in healthy normolipidemic men with early asymptomatic atherosclerosis. *Arterioscler Thromb Vasc Biol.* 2002;22:1470–1474.
29. Bischoff A, Czyborra P, Fetscher C, Meyer Zu Heringdorf D, Jakobs KH, Michel MC. Sphingosine-1-phosphate and sphingosylphosphorylcholine constrict renal and mesenteric microvessels in vitro. *Br J Pharmacol.* 2000;130:1871–1877.
30. Tosaka M, Okajima F, Hashiba Y, Saito N, Nagano T, Watanabe T, Kimura T, Sasaki T. Sphingosine 1-phosphate contracts canine basilar arteries in vitro and in vivo: possible role in pathogenesis of cerebral vasospasm. *Stroke.* 2001;32:2913–2919.
31. Shirao S, Kashiwagi S, Sato M, Miwa S, Nakao F, Kurokawa T, Todoroki-Ikeda N, Mogami K, Mizukami Y, Kuriyama S, Haze K, Suzuki M, Kobayashi S. Sphingosylphosphorylcholine is a novel messenger for Rho-kinase-mediated Ca2+ sensitization in the bovine cerebral artery: unimportant role for protein kinase C. *Circ Res.* 2002;91:112–119.

Long-Term Inhibition of Rho-Kinase Suppresses Neointimal Formation After Stent Implantation in Porcine Coronary Arteries: Involvement of Multiple Mechanisms

Yasuharu Matsumoto, Toyokazu Uwatoku, Keiji Oi, Kohtaro Abe, Tsuyoshi Hattori, Kunio Morishige, Yasuhiro Eto, Yoshihiro Fukumoto, Kei-ichiro Nakamura, Yosaburo Shibata, Takehisa Matsuda, Akira Takeshita, Hiroaki Shimokawa

Objective—We recently demonstrated that Rho-kinase, an effector of the small GTPase Rho, is substantially involved in the pathogenesis of arteriosclerosis. In this study, we examined whether Rho-kinase is also involved in in-stent restenosis and if so, what mechanism is involved.

Methods and Results—Pigs underwent stent implantation in the left coronary artery with or without administration of fasudil (30 mg/kg per day orally), a specific Rho-kinase inhibitor, starting 2 days before the procedure for a duration of 4 weeks. On day 28, reductions in coronary diameter and neointimal formation associated with macrophage accumulation, collagen deposition, and transforming growth factor (TGF)-β1 expression were noted at the stent site, and all were significantly suppressed by fasudil. On day 7, fasudil significantly increased the frequency of TUNEL-positive apoptotic cells, while it tended to reduce that of bromodeoxyuridine-positive proliferating cells in the neointima. Western blot analysis on day 7 demonstrated that phosphorylations of the ezrin/radixin/moesin family (a marker of Rho-kinase activity in vivo) and protein expression of monocyte chemoattractant protein-1and bcl-2 were upregulated at the stent site and were significantly suppressed by fasudil.

Conclusions—These results indicate that long-term inhibition of Rho-kinase suppresses in-stent neointimal formation by multiple mechanisms, including reduced vascular inflammation, enhanced apoptosis, and decreased collagen deposition. (***Arterioscler Thromb Vasc Biol.* 2004;24:181-186.**)

Key Words: Rho-kinase ■ stents ■ inflammation ■ apoptosis ■ collagen

Although the use of stents has dramatically increased in interventional cardiology, in-stent restenosis continues to be a serious problem and is more troublesome when it occurs.[1,2] Furthermore, pharmacological approaches have generally been unsuccessful in suppressing in-stent restenosis except for a recent promising outcome with a drug-eluting stent.[3,4] However, late neointimal catch-up remains a potential adverse outcome with the stent-based drug delivery.[5] More recently, extracellular matrix accumulation has been recognized as a very important component of in-stent restenosis in the chronic phase after stent implantation.[6] Since drug-eluting stents have several limitations for a defined period of time with kinetics and are expensive, there may become a need for systemic therapies to maintain neointimal inhibition, including matrix metabolism.[7,8]

Accumulating evidence has demonstrated that Rho-kinase, an effector of the small GTPase Rho, plays an important role in adhesion, migration, proliferation, and cytokinesis of vascular smooth muscle cells (VSMCs) and other vascular wall cells.[9–11] Rho-kinase is substantially involved in the signal transduction initiated by angiotensin II,[12] platelet-derived growth factor (PDGF),[13] thrombin,[14] and endothelin-1,[15] all of which may play an important role in the pathogenesis of restenosis,[16] especially in that of in-stent restenosis.[17–20]

We recently demonstrated that neointimal formation after balloon injury was significantly inhibited by in vivo gene transfer of dominant-negative Rho-kinase in porcine femoral arteries.[21] A similar finding was also noted in the rat carotid artery with Rho-kinase inhibitor Y-27632, although the relative contribution of inhibition of VSMC proliferation and enhancement of VSMC apoptosis to the inhibitory effect of a Rho-kinase inhibitor remains to be elucidated.[22,23] Furthermore, involvement of Rho-kinase in the extracellular matrix

Received July 25, 2003; revision accepted October 20, 2003.

From the Department of Cardiovascular Medicine (Y.M., H.S., T.U., K.A., K.O., T.H. K.M., Y.E., Y.F., A.T.), the Department of Biomedical Engineering (T.M.), and the Department of Developmental Molecular Anatomy (K.N., Y.S.), Kyushu University Graduate School of Medical Sciences, Fukuoka, Japan.

Consulting Editor for this article was Alan M. Fogelman, MD, Professor of Medicine and Executive Chair, Departments of Medicine and Cardiology, UCLA School of Medicine, Los Angeles, CA.

Correspondence to Hiroaki Shimokawa, MD, PhD, Department of Cardiovascular Medicine, Kyushu University Graduate School of Medical Sciences, 3-1-1 Maidashi, Higashi-ku, Fukuoka 812-8582, Japan. E-mail shimo@cardiol.med.kyushu-u.ac.jp.

Arterioscler Thromb Vasc Biol. is available at http://www.atvbaha.org DOI: 10.1161/01.ATV.0000105053.46994.5B

deposition, especially that of collagen, a major component of the neointima,[6] remains unknown. There are also some differences in the restenosis mechanisms between balloon angioplasty and stent implantation.[24–29]

In the present study, we examined whether long-term inhibition of Rho-kinase suppresses in-stent restenosis in porcine coronary arteries, and if so, what mechanism is involved. For this purpose, we used long-term oral treatment with fasudil, which we found is metabolized to hydroxyfasudil, a specific Rho-kinase inhibitor, after oral administration.[30]

Materials and Methods

This study was reviewed and approved by the Ethical Committee on the Animal Experiments of the Kyushu University Graduate School of Medical Sciences.

Animal Preparation

Thirty-four domestic male pigs (Kyudo, Tosu, Japan; aged 2 to 3 months and weighing 25 to 30 kg) were used. They were divided into 2 groups: the control group was treated with aspirin (325 mg/d) and ticlopidine (500 mg/d) alone (n=17) and the fasudil group with oral administration of fasudil (30 mg/kg per day, Asahi Kasei Company) in addition to the antiplatelet therapy (n=17). The oral administration of fasudil was started 2 days before the procedure and continued until the follow-up period. We performed coronary angiography, intravascular ultrasound (IVUS) imaging, and histological study at 4 weeks (n=6 each). We performed immunostaining for bromodeoxyuridine (BrdU) and terminal deoxynucleotidyl transferase-mediated dUTP nick end-labeling (TUNEL) (n=5 each), and Western blot analysis for substrates of Rho-kinase at 1 week (n=6 each).

Stent Implantation

Nitroglycerin (10 μg/kg IC) was administered prior to angiography. A stainless-steel stent (3.0×18 mm, Multi-Link TRISTAR, Guidant) was implanted to either the left anterior descending (LAD) or the left circumflex coronary (LCx) arteries.[31] A segment with a mean coronary diameter of 2.3 mm was selected by using quantitative coronary angiography with a stent-to-artery ratio of approximately 1.3. A balloon catheter mounted with a stent was then advanced to the pre-selected coronary segments for deployment over a standard guide wire in a blind manner without knowledge about the fasudil treatment. The balloon catheter was inflated at 8 atm for 30 seconds once and was then slowly withdrawn, leaving the stent in place.[31]

Coronary Angiography

Left coronary angiography was performed before, immediately after, and 4 weeks after the stent implantation. Among the 12 animals that underwent angiography, 4 received a stent for LAD and 2 for LCx in the control group, while in the fasudil group, 3 received a stent for LAD and 3 for LCx. A preshaped Judkins catheter was inserted into the right or left carotid artery, and coronary angiography in a left anterior oblique view was performed.[31,32] Arterial pressure, heart rate, and ECG were continuously monitored and recorded on a recorder.

Left coronary angiography was performed in a left anterior oblique projection.[31,32] The measured coronary luminal diameters included mean reference diameter [(proximal + distal) reference diameters/2], mean diameter of the stent site at full expansion, stent-to-artery ratio [(2/1)], and minimal diameter of the stent site at follow-up.[31]

Coronary IVUS

To assess the extent of neointimal formation in vivo, we performed IVUS 4 weeks after the stent implantation, as previously described.[31]

Histopathological Study

For histological analysis, the heart was excised 4 weeks after stent implantation; the left coronary artery was perfused with 10% formalin at 120 mm Hg and fixed for 24 hours. The dissected whole artery was embedded in methylmethacrylate, leaving the stent wires intact to minimize potential artifacts from cutting the wires.[8] After polymerization, stented segments were cut into 3 blocks (proximal, middle, and distal portion) using a rotating saw with diamond edge. The blocks were cut into thin sections (4 to 5 μm) with tungsten carbide blades using a microtome (Leica). The sections were then stained with van Gieson elastic stains. Morphometric analysis of the neointima from photomicrographs was performed for vessel injury score and neointimal area, which was determined by subtracting the lumen area from the area encircled by the internal elastic lamina.[31,33] Mean value of the injury score and neointimal area from the 3 blocks was used for analysis.

Immunohistochemistry

Immunostaining was performed with a specifically designed kit with a tyramide signal amplification (Dako). The antibodies used in this study included monoclonal antibodies to human macrophages (AM-3K, Transgenic) and human α-smooth muscle actin (1A4, Dako), polyclonal antibodies to transforming growth factor (TGF)-β1 (Santa Cruz Biotechnology), and Dolichos biflorus agglutinin for porcine endothelium (Sigma),[34] and nonimmune mouse IgG (Dako). We semi-quantitatively assessed the extent of macrophage accumulation using a conventional scale (0, no cells; 1, scattered cells; 2, focal deposits; and 3, diffuse intense infiltration)[26] and that of re-endothelialization as the percentage of circumference covered by the endothelium (1, <25%; 2, 25% to 75%; and 3, >75%).[4]

Proliferation and Apoptosis

A segment 2 to 3 mm long was cut from the midportion of the stented artery using fine scissors. Stent wires were carefully removed under a dissecting microscope before paraffin embedding.[31] The sections were subjected to BrdU and TUNEL stainings to identify proliferating and apoptotic cells, respectively. BrdU (50 mg/kg) was intravenously injected three times at 24, 16, and 8 hours before necropsy; BrdU-positive cells were detected by the LSAB method and counterstained with hematoxylin.[35] Apoptotic cells were detected with an apoptosis kit (Wako) with porcine small intestine as a positive control. A total cell number and a number of BrdU-positive and TUNEL-positive cells in high-power field were counted in 3 randomly selected fields of each section.[31] A number of BrdU-positive and TUNEL-positive cells were expressed as BrdU index and TUNEL index (BrdU- or TUNEL-positive cells/total cells ×100), respectively.[23]

Collagen Deposition

Collagen deposition was measured on the entire neointima 4 weeks after stent implantation when it became evident. To avoid color balance variation, sirius red staining of all sections was performed at the same time. Then, once a standard for the particular slide/section was set by polarization microscopy, all the sections from the different groups of animals were photographed with the same strength of light by digital image capture.[36]

Western Blot Analysis

Stented coronary segments were subjected to SDS-PAGE immunoblot analysis at 1 week, as described previously.[32] Phosphorylation of the ezrin/radixin/moesin (ERM) substrates of Rho-kinase was measured, using a rabbit polyclonal antibody to phosphorylated human moesin (Thr558), which also binds to phosphorylated ezrin (Thr567) and radixin (Thr564). Monocyte chemoattractant protein (MCP)-1 (R&D Systems) and bcl-2 (Roche Diagnostics) were also evaluated.

Statistical Analysis

Results are expressed as means±SEM. Throughout the text and figures, n represents the number of animals tested. Comparison

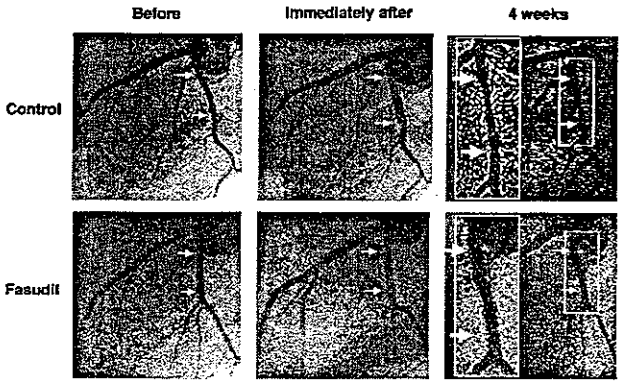

Figure 1. Coronary angiograms before, immediately after, and 4 weeks after stent implantation in the control and fasudil groups. The arrows indicate the proximal and distal portion of the stented coronary artery. High-resolution images are inserted.

between the control and the fasudil groups was performed by an unpaired, two-tailed t test. Multiple comparisons were made by analysis of variance followed by Scheffe post hoc test. A probability value of <0.05 was considered to be statistically significant.

Results

Coronary Angiography

Before stent implantation, there was no significant difference in coronary diameter (mm) between the control (2.33±0.31) and the fasudil (2.31±0.03) groups (Figure 1 and Figure I, available online at http://atvb.ahajournals.org). Similarly, there was no significant difference in the diameter (mm) at full stent expansion (2.95±0.02 versus 2.97±0.02) or stent-to-artery ratio (1.27±0.02 versus 1.29±0.02) between the 2 groups. Four weeks after the stent implantation, coronary diameter (mm) at the stent site was significantly decreased in the control group (1.65±0.11) but remained unchanged in the fasudil group (2.23±0.12) (Figure 1 and Figure I). There was no significant change in mean arterial pressure throughout the experiment in both groups (data not shown).

IVUS Analysis

IVUS analysis demonstrated that the extent of neointimal formation (as expressed by percentage of neointimal area to the area covered by stent) was significantly less in the fasudil group (36.6±3.7) than in the control group (50.2±4.7) ($P<0.05$).

Histology

Neointimal area (mm^2) was significantly less in the fasudil group (2.2±0.2) than in the control group (3.1±0.3) ($P<0.05$), while injury score was comparable between the control (1.13±0.11) and the fasudil (1.20±0.09) groups (Figure 2). Endothelialization score was also comparable between the control (2.8±0.2) and the fasudil (2.8±0.2) groups.

Rho-Kinase Activity

The extent of ERM family phosphorylation was significantly increased at the stent site in the control group and significantly suppressed in the fasudil group (Figure 3).

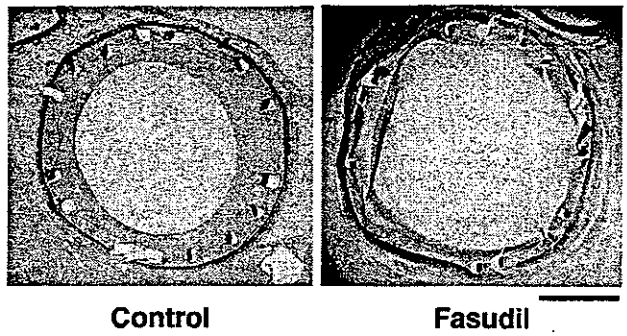

Figure 2. Photomicrographs (van Gieson elastic staining) of stented coronary segments 4 weeks after stent implantation in the control and the fasudil groups. Calibration, 1 mm.

Vascular Inflammation

At 4 weeks, macrophage accumulation was noted in the neointima and to a greater extent, in the adventitia in the control group and was significantly suppressed in the fasudil group (Figure 4 and Figure II, available online at http://atvb.ahajournals.org). At 1 week, MCP-1 protein expression increased and was again significantly reduced by fasudil (Figure III, available online at http://atvb.ahajournals.org).

Proliferation and Apoptosis

In the intact artery, neither BrdU-positive nor TUNEL-positive cells were detected in the intima or the media (data not shown). Although statistically insignificant, BrdU index (%) tended to be reduced in the fasudil group (23.2±2.0) compared with the control group (33.2±5.0) at 1 week ($P=0.10$). In contrast, TUNEL index at 1 week was significantly increased in the fasudil group (55.5±5.4) compared with the control group (33.8±4.6) ($P<0.05$) (Figure 5). Bcl-2 protein expression increased in the control group, which was significantly downregu-

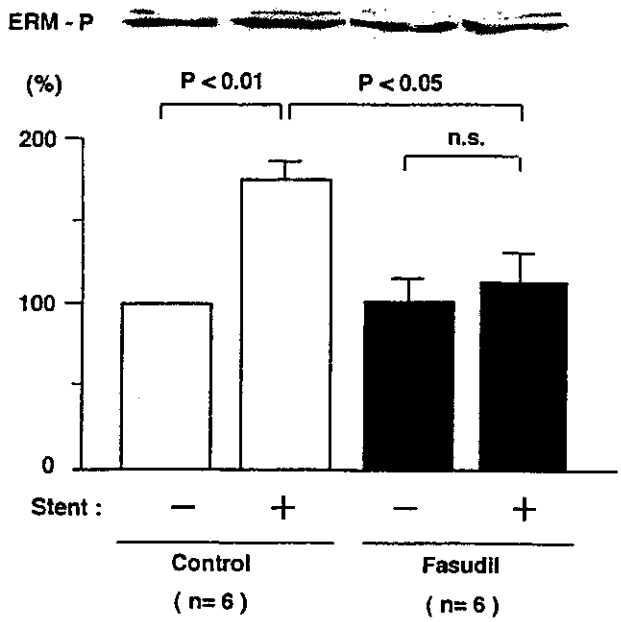

Figure 3. Western blot analysis for phosphorylated ERM (a marker of Rho-kinase activity) in porcine coronary segments with and without stent implantation in the control and the fasudil groups. Results are expressed as means±SEM.

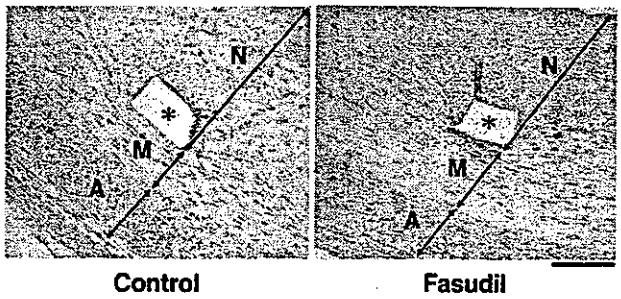

Figure 4. Inhibitory effects of fasudil on macrophage accumulation at the stented porcine coronary arteries. Photomicrographs show immunostaining for macrophages 4 weeks after stent implantation in the control and the fasudil groups. Calibration, 100 μm. N indicates neointima; M, media; A, adventitia. *Stent strut.

lated by the fasudil treatment (Figure IV, available online at http://atvb.ahajournals.org).

Collagen Deposition

Picrosirius red polarization showed that neointimal collagen content (%) was significantly less in the fasudil group (24.1±3.1) than in the control group (43.6±3.2) ($P<0.01$) (Figure 6). Immunostaining for TGF-β1 revealed reduced TGF-β1 immunoreactivity in the fasudil group rather than in the control group (Figure 6).

Side Effects

In the present study, no appreciable side effects, such as weight loss, diarrhea, or blood abnormalities, were noted in the fasudil group (data not shown).

Discussion

The novel findings of the present study were: (1) Rho-kinase activity was enhanced at the stent implantation site associated with neointimal formation and (2) long-term inhibition of Rho-kinase with fasudil significantly suppressed the neointimal formation by multiple mechanisms, including inhibition of vascular inflammation, enhanced apoptosis, and reduced collagen deposition (Figure V, available online at http://atvb.ahajournals.org). To the best of our knowledge, this is the first report that demonstrates the involvement of Rho-kinase in in-stent restenosis and

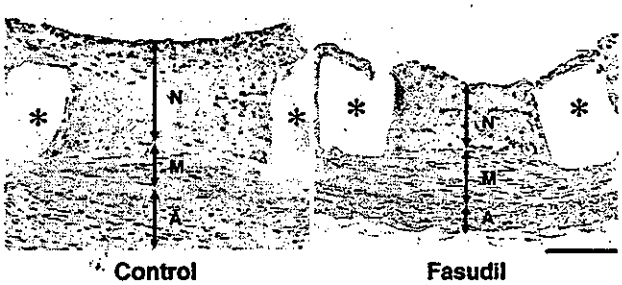

Figure 5. Proapoptotic effects of fasudil at the stented porcine coronary segments at 1 week after stent implantation. Photomicrographs show TUNEL-positive cells. More TUNEL-positive cells were noted in the neointima in the fasudil group than in the control group. Calibration, 100 μm. N indicates neointima; M, media; A, adventitia. *Stent strut.

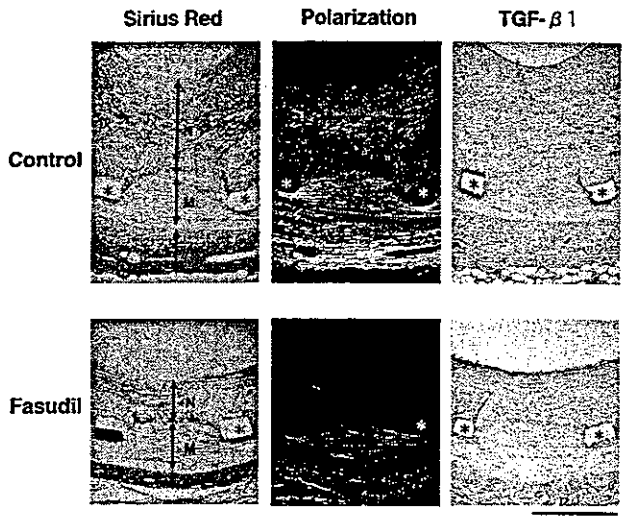

Figure 6. Inhibitory effects of fasudil on collagen deposition at the stented porcine coronary segments at 4 weeks after stent implantation. Sirius red stainings without (left) and with (middle) polarized light show more thickened neointima and abundant collagen deposition, respectively, in the control group compared with the fasudil group. Right, TGF-β1 immunoreactivity was detected in the neointima and the adventitia in the control group and was almost undetectable in the fasudil group. Calibration, 400 μm. N indicates neointima; M, media; A, adventitia. *Stent strut.

thereby the potential usefulness of a Rho-kinase inhibitor to prevent the disorder.

Increased Rho-Kinase Activity by Stent Implantation

We previously demonstrated that both expression and activity of Rho-kinase increase after balloon injury[21] and on stimulation by an inflammatory cytokine[9] in pigs in vivo. The present study also demonstrated that stent implantation increased Rho-kinase activity. Recent studies in vitro have shown that Rho-kinase and its substrates mediate actin cytoskeleton organization, cell adhesion and migration, and cytokinesis,[9–11] all of which may be involved in in-stent neointimal formation. Although a molecular mechanism for the upregulation of Rho-kinase by stent implantation remains to be elucidated, it has recently been demonstrated that various vasoactive factors enhance Rho-kinase activity in vitro.[9] Indeed, we have recently demonstrated that Rho-kinase plays an important role in angiotensin II-induced MCP-1 expression in cultured rat VSMCs.[12] Various growth factors (eg, PDGF) and cytokines, angiotensin-II, endothelin-1, and thrombin may all be involved in restenosis after angioplasty.[16–20] Importantly, all of them could upregulate Rho-kinase.[12–15] Thus, it is highly possible that Rho-kinase plays an important role in the pathogenesis of in-stent restenosis (Figure V).

Mechanism for the Inhibitory Effect of Fasudil on Neointimal Formation After Stent Implantation

The present study demonstrated that multiple mechanisms are involved in the inhibitory effect of fasudil on neointimal formation after stent implantation, including inhibition of

vascular inflammation, enhanced apoptosis, and reduced collagen deposition.

In-stent restenosis is characterized by prolonged and pronounced inflammation.[26,37–39] In this study, the long-term treatment with fasudil suppressed macrophage accumulation, not only around stent struts but also in the adventitia. We previously demonstrated that long-term treatment with fasudil significantly suppresses macrophage accumulation at the adventitia and subsequent coronary vascular lesion formation in porcine coronary arteries in vivo.[40] Two mechanisms may be involved for the anti-inflammatory effect of fasudil. First, fasudil may directly inhibit macrophage chemotaxis.[41] Second, fasudil may inhibit the expression of proinflammatory molecules such as MCP-1.[12] Importantly, the inhibitory effect of fasudil on the MCP-1 expression at the stent site (70% reduction) is equivalent to that of sirolimus-coated stent.[4] It is thus highly possible that reduced MCP-1 expression resulted in decreased macrophage accumulation at 4 weeks after stent implantation.

In the present study, fasudil significantly enhanced apoptosis, a consistent finding with a previous study.[23] However, the molecular mechanism for the proapoptotic effect of fasudil remains to be elucidated. In the present study, we demonstrated that downregulation of anti-apoptotic protein bcl-2 is involved in the proapoptotic effect of fasudil. Although statistically insignificant, fasudil also tended to reduce cellular proliferation. While it has been controversial whether an antiproliferative effect is involved in the antiatherogenic effect of a Rho-kinase inhibitor,[22,23] the present results suggest that such effect may not play a central role in the present porcine model, although this point remains to be examined in a future study. Fasudil did not affect the extent of re-endothelialization in vivo, a consistent finding with a previous report on Y-27632.[23] Thus, it is suggested that Rho-kinase is not involved in endothelial regeneration after vascular injury.

Finally, the importance of extracellular matrix formation is recognized as a key component of in-stent restenosis.[6] Stent implantation causes a significant increase in collagen synthesis and TGF-β expression compared with balloon angioplasty alone.[27,28] In the present study, we demonstrated the abundant collagen deposition associated with TGF-β1 expression in all layers of stented coronary arteries. TGF-β is one of the most potent stimuli for collagen synthesis and may contribute to the formation of restenotic lesions.[16] A substantial portion of the neointima consists of matrix rather than cells.[6] Thus, a strategy to inhibit TGF-β may be useful in preventing in-stent neointimal formation.[28] In this study, we were able to demonstrate for the first time that long-term treatment with fasudil significantly suppresses collagen deposition in the neointimal lesion after stent implantation due, at least in part, to the inhibition of TGF-β1 expression.

Possible Side Effects of Fasudil

In the present study, no appreciable side effects were observed in the fasudil group, and fasudil had no effects on arterial pressure or nonstented coronary artery. We have recently demonstrated that fasudil is well tolerated without any serious side effects in patients with angina.[42] Thus, fasudil may be a safe drug, although caution should be made when used clinically.

Limitations of the Study

Several limitations of the present study should be mentioned. First, the present study was performed in the normal porcine coronary artery without preexisting intimal thickening. Thus, the inhibitory effects of fasudil need to be confirmed in animal models with atherosclerotic coronary lesions. Second, cell-specific Rho-kinase expression was not examined. However, based on our recent findings[9,40] and the present results with stainings for BrdU, TUNEL and macrophages, we consider that Rho-kinase was expressed mainly in macrophages and VSMCs. Third, although we confirmed the inhibitory effect of fasudil (hydroxyfasudil) on Rho-kinase in the present study,[30] other unknown effects of this agent might be involved. Fourth, it remains to be examined how long fasudil should be continued to prevent neointimal formation after coronary stenting or whether lesion development is permanently suppressed by some period of treatment with fasudil. Finally, there are some differences in the mechanism between atherosclerosis and restenosis, including severity of injury, time course of the response, cellular/extracellular elements, and relation to lipids.[43] Thus, an agent that may have beneficial effects in atherosclerosis may not be equally effective in the prevention of in-stent restenosis.

In summary, the present results indicate that long-term inhibition of Rho-kinase suppresses in-stent restenosis by multiple mechanisms, suggesting the potential usefulness of a Rho-kinase inhibitor to prevent the disorder (Figure V).

Acknowledgments

We thank M. Sonoda, E. Gunshima, I. Kunihiro for excellent technical assistance, and Asahi Kasei Co. (Tokyo, Japan) for providing fasudil. This study was supported in part by the grants-in-aid from the Japanese Ministry of Education, Culture, Sports, Science and Technology, Tokyo, Japan (Nos. 12032215, 12470158, 12877114, 13307024, 13557068) and the Program for Promotion of Fundamental Studies in Health Sciences of the Organization for Pharmaceutical Safety and Research of Japan.

References

1. Topol EJ, Serruys PW. Frontiers in interventional cardiology. *Circulation* 1998;98:1802–1820.
2. Lowe HC, Oesterle SN, Khachigian LM. Coronary in-stent restenosis: current status and future strategies. *J Am Coll Cardiol.* 2002;39:183–193.
3. Morice M, Serruys PW, Sousa JE, Fajadet J, Hayashi EB, Perin M, Colombo A, Schuler M, Barragan P, Guagliumi G, Molnar F, Falotico R. A randomized comparison of a sirolimus-eluting stent with a standard stent for coronary revascularization. *N Engl J Med.* 2002;346:1773–1780.
4. Suzuki T, Kopia G, Hayashi S, Bailey LR, Llanos G, Wilensky R, Klugherz BD, Papandreou G, Narayan P, Leon MB, Yeung AC, Tio F, Tsao PS, Falotico R, Carter AJ. Stent-based delivery of sirolimus reduces neointimal formation in a porcine coronary model. *Circulation* 2001;104:1188–1193.
5. Liistro F, Stankovic G, Di Mario C, Takagi T, Chieffo A, Moshiri S, Montorfano M, Carlino M, Briguori C, Pagnotta P, Albiero R, Corvaja N, Colombo A. First clinical experience with a paclitaxel derivate-eluting polymer stent system implantation for in-stent restenosis: immediate and long-term clinical and angiographic outcome. *Circulation* 2002;105:1883–1886.
6. Chung I-M, Gold HK, Schwartz SM, Ikari Y, Reidy MA, Wight TN. Enhanced extracellular matrix accumulation in restenosis of coronary arteries after stent deployment. *J Am Coll Cardiol.* 2002;40:2072–2081.

7. Faxon DP. Systemic drug therapy for restenosis. *Circulation* 2002;106: 2296–2298.
8. Farb A, John M, Acampado E, Kolodgie FD, Prescott MF, Virmani R. Oral everolimus inhibits in-stent neointimal growth. *Circulation* 2002; 106:2379–2384.
9. Shimokawa H. Rho-kinase as a novel therapeutic target in treatment of cardiovascular diseases. *J Cardiovascular Phrmacol.* 2002;39:319–327.
10. Fukata Y, Amano M, Kaibuchi K. Rho-Rho-kinase pathway in smooth muscle contraction and cytoskeletal reorganization of non-muscle cells. *Trends Pharmacol Sci.* 2001;22:32–39.
11. van Nieuw Amerongen GP, van Hinsbergh VWM. Cytoskeletal effects of rho-like small guanine nucleotide-binding proteins in the vascular system. *Arterioscler Thromb Vasc Biol.* 2001;21:300–311.
12. Funakoshi Y, Ichiki T, Shimokawa H, Egashira K, Takeda K, Kaibuchi K, Takeya M, Yoshimura T, Takeshita A. Rho-kinase mediates angiotensin II-induced monocyte chemoattractant protein-1 expression in rat vascular smooth muscle cells. *Hypertension* 2001;38:100–104.
13. Kishi H, Bao J, Kohama K. Inhibitory effects of ML-9, wortmannin, and Y-27632 on the chemotaxis of vascular smooth muscle cells in response to platelet-derived growth factor-BB. *J Biochem.* 2000;128:719–722.
14. Seasholtz TM, Majumdar M, Kaplan DD, Brown JH. Rho and Rho kinase mediate thrombin-stimulated vascular smooth muscle cell DNA synthesis and migration. *Circ Res.* 1999;84:1186–1193.
15. Yamamoto Y, Ikegaki I, Sasaki Y, Uchida T. The protein kinase inhibitor fasudil protects against ischemic myocardial injury induced by endothelin-1 in the rabbit. *J Cardiovasc Pharmacol.* 2000;35:203–211.
16. Libby P, Edelman E. Restenosis: Involvement of Growth Factors and Cytokines. In: Topol EJ, eds. *Textbook of Interventional Cardiology.* 3rd edition. Philadelphia, Pa: Saunders; 1999: 346–357.
17. Peters S, Gotting B, Trummel M, Rust H, Brattstrom A. Valsartan for prevention of restenosis after stenting of type B2/C lesions: the VAL-PREST trial. *J Invasive Cardiol* 2001;13:93–97.
18. Brasen JH, Kivela A, Roser K, Rissanen TT, Niemi M, Luft FC, Donath K, Yla-Herttuala S. Angiogenesis, vascular endothelial growth factor and platelet-derived growth factor-BB expression, iron deposition, and oxidation-specific epitopes in stented human coronary arteries. *Arterioscler Thromb Vasc Biol.* 2001;21:1720–1726.
19. Schwartz RS, Holder DJ, Holmes DR, Veinot JP, Camrud AR, Jorgenson MA, Johnson RG. Neointimal thickening after severe coronary artery injury is limited by a short-term administration of a factor Xa inhibitor. Results in a porcine model. *Circulation* 1996;93:1542–1548.
20. McKenna CJ, Burke SE, Opgenorth TJ, Padley RJ, Camrud LJ, Camrud AR, Johnson J, Carlson PJ, Lerman A, Holmes DR Jr., Schwartz RS. Selective ET(A) receptor antagonism reduces neointimal hyperplasia in a porcine coronary stent model. *Circulation* 1998;97:2551–2556.
21. Eto Y, Shimokawa H, Hiroki J, Morishige K, Kandabashi T, Matsumoto Y, Amano M, Hoshijima M, Kaibuchi K, Takeshita A. Gene transfer of dominant negative Rho kinase suppresses neointimal formation after balloon injury in pigs. *Am J Physiol.* 2000;278:H1744–1750.
22. Sawada N, Itoh H, Ueyama K, Yamashita J, Doi K, Chun TH, Inoue M, Masatsugu K, Saito T, Fukunaga Y, Sakaguchi S, Arai H, Ohno N, Komeda M, Nakao K. Inhibition of Rho-associated kinase results in suppression of neointimal formation of balloon-injured arteries. *Circulation* 2000;101:2030–2033.
23. Shibata R, Kai H, Seki Y, Kato S, Morimatsu M, Kaibuchi K, Imaizumi T. Role of Rho-associated kinase in neointima formation after vascular injury. *Circulation* 2001;103:284–289.
24. Karas SP, Gravanis MB, Santoian EC, Robinson KA, Anderberg KA, King SB III. Coronary intimal proliferation after balloon injury and stenting in swine: animal model of restenosis. *J Am Coll Cardiol.* 1992; 20:467–474.
25. Mintz GS, Hoffman R, Mehran R, Hong MK, Waksman R, Pichard AD, Kent KM, Satler LF, Leon MB. In-stent Restenosis: Mechanisms, Definitions, and Treatment. In: Stack RS, Roubin GS, O'Neill W, eds. *Interventional Cardiovascular Medicine:Principles and Practice.* 2nd edition. Philadelphia, Pa: Churchill Livingstone; 2002: 782–791.
26. Horvath C, Welt FGP, Nedelman M, Rao P, Rogers C. Targeting CCR2 or CD18 inhibits experimental in-stent restenosis in primates. *Circ Res.* 2002;90:488–494.
27. Li C, Cantor WJ, Nili N, Robinson R, Fenkell L, Tran YL, Whittingham HA, Tsui W, Cheema AN, Sparkes JD, Pritzker K, Levy DE, Strauss BH. Arterial repair after stenting and the effects of GM6001, a matrix metalloproteinase inhibitor. *J Am Coll Cardiol.* 2002;39:1852–1858.
28. Chamberlain J. Transforming growth factor-beta: a promising target for anti-stenosis therapy. *Cardiovasc Drug Rev* 2001;19:329–44.
29. van Beusekom HM, Whelan DM, Hofma SH, Krabbendam SC, van Hinsbergh VWM, Verdouw PD, van der Giessen WJ. Long-term endothelial dysfunction is more pronounced after stenting than after balloon angioplasty in porcine coronary arteries. *J Am Coll Cardiol.* 1998;32: 1109–1117.
30. Shimokawa H, Seto M, Katsumata N, Amano M, Kozai T, Yamawaki T, Kuwata K, Kandabashi T, Egashira K, Ikegaki I, Asano T, Kaibuchi K, Takeshita A. Rho-kinase-mediated pathway induces enhanced myosin light chain phosphorylations in a swine model of coronary artery spasm. *Cardiovasc Res.* 1999;43:1029–1039.
31. Matsumoto M, Shimokawa H, Morishige K, Eto Y, Takeshita A. Reduction in neointimal formation with a stent coated with multiple layers of releasable heparin in porcine coronary arteries. *J Cardiovasc Pharmacol.* 2002;39:513–522.
32. Morishige K, Shimokawa H, Eto Y, Kandabashi T, Miyata K, Matsumoto Y, Hoshijima M, Kaibuchi K, Takeshita A. Adenovirus-mediated transfer of dominant-negative Rho-kinase induces a regression of coronary arteriosclerosis in pigs in vivo. *Arterioscler Thromb Vasc Biol.* 2001;21: 548–554.
33. Schwartz RS, Huber KC, Murphy JG, Edwards WD, Camrud AR, Vlietstra RE, Holmes DR. Restenosis and the proportional neointimal response to coronary artery injury: results in a porcine model. *J Am Coll Cardiol.* 1992;19:267–274.
34. Mills AN, Haworth SG. Changes in lectin-binding patterns in the developing pulmonary vasculature of the pig lung. *J Pathol.* 1986;149: 191–199.
35. Scott NA, Cipolla GD, Ross CE, Dunn B, Martin FH, Simonet L, Wilcox JN. Identification of a potential role for the adventitia in vascular lesion formation after balloon overstretch injury of porcine coronary arteries. *Circulation* 1996;93:2178–2187.
36. Fukumoto Y, Libby P, Rabkin E, Hill CC, Enomoto M, Hirouchi Y, Shiomi M, Aikawa M. Statins alter smooth muscle cell accumulation and collagen content in established atheroma of watanabe heritable hyperlipidemic rabbits. *Circulation* 2001;103:993–999.
37. Komowski R, Hong MK, Fermin OT, Bramwell O, Wu H, Leon MB. In-stent restenosis: contributions of inflammatory responses and arterial injury to neointimal hyperplasia. *J Am Coll Cardiol.* 1998;31:224–230.
38. Komatsu R, Ueda M, Naruko T, Kojima A, Becker AE. Neointimal tissue response at sites of coronary stenting in humans. *Circulation* 1998;98: 224–233.
39. Farb A, Weber DK, Kolodgie FD, Burke AP, Virmani R. Morphological predictors of restenosis after coronary stenting in humans. *Circulation* 2002;105:2974–2980.
40. Miyata K, Shimokawa H, Kandabashi T, Higo T, Morishige K, Eto Y, Egashira K, Kaibuchi K, Takeshita A. Rho-kinase is involved in macrophage-mediated formation of coronary vascular lesions in pigs in vivo. *Arterioscler Thromb Vasc Biol.* 2000;20:2351–2358.
41. Ashida N, Arai H, Yamasaki M, Kita T. Distinct signaling pathways for MCP-1-dependent integrin activation and chemotaxis. *J Biol Chem.* 2001; 276:16555–16560.
42. Shimokawa H, Hiramori K, Iinuma H, Hosoda S, Kishida H, Osada H, Katagiri T, Yamauchi K, Yui Y, Minamino T, Nakashima M, Kato K. Anti-anginal effect of fasudil, a Rho-kinase inhibitor, in patients with stable effort angina: a multicenter study. *J Cardiovasc Pharmacol.* 2002; 40:751–761.
43. Libby P, Simon DI, Rogers C. Inflammation and Arterial Injury. In: Topol EJ, ed. *Textbook of Interventional Cardiology.* 4th edition. Philadelphia, Pa: Saunders; 2003: 381–389.

Intracellular Signal-Responsive Gene Carrier for Cell-Specific Gene Expression

Kenji Kawamura,† Jun Oishi,† Jeong-Hun Kang,‡ Kota Kodama,‡ Tatsuhiko Sonoda,† Masaharu Murata,† Takuro Niidome,† and Yoshiki Katayama*,†,‡

Department of Applied Chemistry, Faculty of Engineering, Kyushu University, Hakozaki, Higashi-ku, Fukuoka 812-8581, and CREST, Japan Science and Technology Agency, 4-1-8 Honcho, Kawaguchi-shi, Saitama 332-0012, Japan

Received September 28, 2004; Revised Manuscript Received November 6, 2004

We designed a peptide−polymer conjugate (CPCCtat) as a novel gene carrier that could control gene expression responding to the intracellular caspase-3 signal. This carrier consists of an uncharged main polymer chain and a cationic peptide side chain, which includes the substrate sequence of caspase-3 and the protein transduction domain sequence of HIV-1 Tat. In the present study, CPCCtat formed a tight complex with DNA through an electrostatic interaction, and in this state the gene expression was totally suppressed. In contrast, the complex disintegrated in the presence of caspase-3 due to cleavage of the cationic portion from CPCCtat. This event led to an activation of gene expression. Our results also indicate that the complex can be delivered into living cells due to the cell-permeable peptide side chain of CPCCtat. This intracellular signal-responsive system with CPCCtat will be useful for the cell-specific gene expression system.

Introduction

Recent progress in genomic research has revealed novel genes related to various diseases and has made it possible to apply them to gene therapies. In fact, 918 protocols have already been carried out in clinical trials.[1] To further generalize gene therapy, however, it is necessary for expression of the delivered gene to be activated only in the target cell to avoid side effects. In fact, some serious side effects in gene therapy have been reported due to nonspecific gene expression in untargeted cells. Thus, many targeting strategies have been investigated in various drug and gene delivery systems.[2−7] These strategies often utilize the interaction between a molecular marker on the cellular surface that is specific to the target disease cells and the ligand molecules attached to the gene carrier. However, this so-called active targeting strategy is sometimes not very successful because the effective molecular markers are not always available. Therefore, the present applications of gene therapy have been restricted to cases that do not require control of the delivered gene expression.

We propose herein a novel strategy that can discriminate normal cells and target cells in gene therapy by focusing on differences in intracellular signals. Living cells possess elaborate molecular reaction cascades, referred to as an intracellular signal transduction system, in individual cells to regulate cellular functions and responses. Hyperactivation of certain intracellular signals is often seen in many diseases.[8−15] Thus, if such unusual intracellular signals could be used to activate the delivered gene, cell-selective control of the delivered gene expression could be achieved. We have previously reported a drug capsule and gene carrier system that releases drug activity or gene expression, respectively, responding to a certain intracellular kinase or protease signal.[16−18] However, the gene carrier reported previously could not deliver DNA into living cells, although these materials worked well in cell-free systems.

In the present study, we designed a novel cell-permeable gene carrier that can activate the delivered gene in response to the intracellular caspase-3 signal, which is a cysteinyl protease and plays an important role in apoptosis. Control of gene expression depending on the activation of intracellular caspase-3 was demonstrated using a cellular sample. We term this approach for gene delivery with cell-signal-specific gene expression D-RECS (drug delivery system responding to cellular signaling).

Materials and Methods

Preparation of the Caspase-3-Responsible Polymer CPCCtat. CPCCtat was synthesized in a manner similar to that described previously.[16,17] Thus, a methacryloyl peptide (6.6 mg, 2.67 μmol) in which the methacryloyl group was attached at the amino terminus of the peptide and the acrylamide (10 mg, 140 μmol) were dissolved in degassed water and allowed to stand at room temperature for 1 h after the addition of ammonium persulfate (1.1 mg, 4.82 μmol) and *N,N,N′,N′*-tetramethylethylenediamine (1.42 μL, 9.48 μmol) as the redox initiator couple. The product was then purified by overnight dialysis against water using a semipermeable membrane bag (with a molecular weight cutoff of 25000), followed by lyophilization to obtain a white powder at 30% yield.

* To whom correspondence should be addressed. E-mail: ykatatcm@mbox.nc.Kyushu-u.ac.jp.
† Kyushu University.
‡ Japan Science and Technology Agency.

10.1021/bm0493887 CCC: $30.25
Published on Web 00/00/0000 PAGE EST: 5.1

Gel Electrophoresis. Linear DNA (1234 bp, 0.1 μg) which was a restriction fragment from pRL-null was dissolved in 2 μL of sterile water. The CPCCtat was then added to the solution at various concentrations. All solutions were diluted to 4.2 μL with sterile water, allowed to stand for 15 min at room temperature, and then analyzed by 1% agarose gel electrophoresis in Tris−borate buffer (pH 8.0). For the caspase-3 reaction, activated caspase-3 (2 U, CHEMICON) was added to each solution, and the resulting solutions were incubated for 90 min at 37 °C before being subjected to gel electrophoresis.

Luciferase Expression in a Cell-Free System. All experiments were performed using a cell-free expression system (T7 S30 extract system for circular DNA, Promega) containing the T7 S30 extract and an amino acid mixture. Luciferase was expressed for 40 min at 37 °C using luciferase-encoding DNA (pRL-CMV). To prepare the CPCCtat−DNA 1:1 complex, the CPCCtat was mixed with the DNA (1 μg) at a concentration in which the ratio of the cationic charge of the CPCCtat (the net charge of each peptide side chain was assumed to be +5) to the phosphate residue in the DNA was 1.0, 15 min before the expression experiment. In the treatment of the 1:1 complex with caspase-3, the solution containing the DNA−CPCCtat complex was preincubated with activated caspase-3 (2 U) for 1.0 h at 37 °C, and 5 μg (10 nmol) of a caspase-3 inhibitor (Ac-DEVD-CHO) was then added before the expression experiment. In the experiment using factor Xa, factor Xa (1 μg) was used instead of caspase-3. In the control experiment, luciferase was expressed using the solution containing 1 μg of the DNA (4.8 nmol/μL as the phosphate residue) without CPCCtat or caspase-3. To monitor the chemiluminescence, 10 μL of the reaction mixture was added to the luciferase assay solution (Promega), and the chemiluminescence was measured using a multilabel counter, ARVO (WALLAC Inc.).

The determination of messenger RNA was performed using an RNA6000 Nano assay kit (Agilent Technologies) and Agilent 2100 bioanalyzer. Typically, an aliquot of the reaction mixture was loaded onto the gel microchip, in which a fluorescent probe for messenger RNA detection had been premixed, and the target messenger RNA was separated with electrophoresis. Then, the target messenger RNA was quantified by comparing its band area with that of marker RNA.

Delivery of the DNA−CPCCtat Complex into NIH 3T3 Cells and Regulation of Gene Expression by Intracellular Apoptotic Signals. NIH 3T3 cells (1×10^4 cells) were seeded into each well of a 96-well microtiter plate and incubated with Dulbecco's modified Eagle's medium (DMEM) supplemented with 10% fetal bovine serum (FBS) at 37 °C under a 5% CO_2 atmosphere. After an overnight incubation, the culture medium was exchanged to OPTI-MEM without serum. The EGFP-encoding DNA−CPCCtat complex at a charge ratio of 1.0 was delivered into the NIH 3T3 cells in the presence or absence of apoptotic stimulation. For the apoptotic stimulation, the cells were pretreated with staurosporin (50 μM). Delivery of the DNA−CPCCtat complex into the NIH 3T3 cells was as follows. pEGFP (0.1 μg) was incubated with the CPCCtat (0.92 mg) in 2 μL of sterile water for 15 min to form the complex. The complex solution was then diluted to 100 μL with OPTI-MEM and added to each well, followed by incubation for 2 h under a 5% CO_2 atmosphere at 37 °C.

Delivery of the CPCCtat−DNA Complex with HVJ-E (Envelope of Hemagglutinating Virus of Japan) and Regulation of Gene Expression Responding to Intracellular Apoptotic Signals. The DNA−CPCCtat complex was transfected into NIH 3T3 cells using GenomONE (HVJ-E) purchased from Ishihara Industries. NIH 3T3 cells (1×10^4 cells) were seeded into each well of a 96-well microtiter plate and incubated in DMEM with 10% FBS at 37 °C under a 5% CO_2 atmosphere. After an overnight incubation, the EGFP-encoding DNA−CPCCtat complex at a charge ratio of 1.0 or 2.0 encapsulated in HVJ-E was delivered into the NIH 3T3 cells. The DNA−CPCCtat complex was encapsulated into HVJ-E according to the protocol recommended by the supplier with slight modification.

In brief, one assay unit (20 μL) of HVJ-E was centrifuged at 10000 rpm for 5 min at 4 °C. After removal of the supernatant, the pellet was suspended in 5 μL of buffer solution. The suspension was mixed with 16 μL of EGFP-encoding DNA−CPCCtat complex solution (0.8 μg of DNA and CPCCtat at a charge ratio of 1.0) and 2.1 μL of reagent B (detergent). The mixture was centrifuged at 10000 rpm for 5 min at 4 °C. After removal of the supernatant, the pellet was suspended with 12.5 μL of buffer solution and then mixed with 5 μL of reagent C (protamine sulfate). Next, 2 μL of this mixture was diluted with OPTI-MEM (with 5% FBS) to 100 μL, and this suspension was added to a well in a 96-well plate. After a 1 h incubation, staurosporine was added to the cultured medium (final concentration 1 μM). The plate was incubated at 37 °C under a 5% CO_2 atmosphere for 15 h, and observed with a confocal laser scan microscope. Preparation of the DNA−CPCCtat complex was described above.

Results and Discussion

Design and Preparation of the Caspase-3-Responsible Polymer CPCCtat. To achieve cell-selective gene expression, we designed a novel polymer that could activate the delivered gene expression responding to the intracellular caspase-3 signal. The polymer CPCCtat (cationic polymer possessing the cleavage site for caspase-3) is a graft-type copolymer that is composed of polyacrylamide for the main chain and cationic peptide for the side chain (Figure 1a). This peptide side chain contains a consensus amino acid sequence, DEVD (anionic), for the selective cleavage site of caspase-3[19] and the protein transduction domain sequence of HIV-1 Tat protein (Tat peptide, GRKKRRQRRRPPQ) for the cationic portion and cell-permeable unit.[20,21] This polymer was obtained in good yield using methacryloyl peptide monomer and acrylamide with radical polymerization. The resulting CPCCtat contained the peptide side chain at a concentration of 0.81 mol % as the monomer unit content, estimated by the results of elemental analysis. CPCCtat forms a stable complex with DNA through an electrostatic interaction, and this complex is taken up by living cells due to the cell-permeable peptide in CPCCtat.

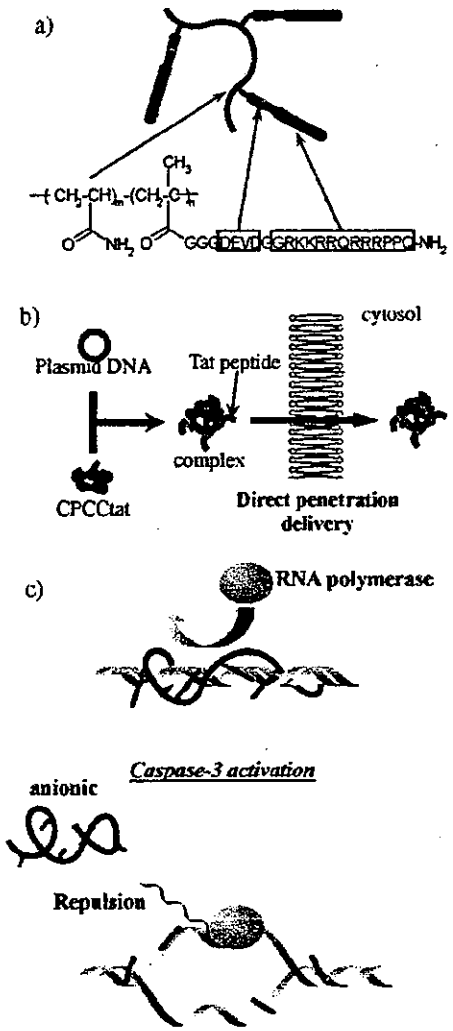

Figure 1. Concept of the gene delivery and gene regulation system with the intracellular caspase-3 signal-responsive polymer CPCCtat. (a) Structure of CPCCtat. CPCCtat consists of acrylamide as the main chain and peptides as the side chain. The pendant peptides include the anionic caspase-3 cleavage site (blue) and a cell-permeable cationic portion (red). (b) Cellular uptake of the CPCCtat–DNA complex. The CPCCtat forms stable complexes with DNA through electrostatic interactions. The protein transduction domain sequence (Tat peptide) of the side chain peptide in CPCCtat then leads the CPCCtat–DNA complex into the cell. (c) Mechanistic scheme of artificial gene regulation responding to caspase-3. When the CPCCtat forms a complex with the DNA, gene expression is suppressed. When the intracellular caspase-3 is activated, the cationic portion of the peptide in the CPCCtat is cleaved with caspase-3. These events cause a disintegration of the complex and release the DNA to activate gene transcription.

Figure 1c shows the concept of gene regulation with the CPCCtat–DNA complex. In the polymer–DNA complex, CPCCtat suppresses the accessibility of RNA polymerase to the DNA strand. In contrast, when the intracellular caspase-3 is continuously activated, this complex is disintegrated due to cleavage of the cationic portion of the peptide side chain from the main polymer chain. In this case, the net charge of the polymer changes from cationic to anionic, and free DNA is released from the polymer–DNA complex by an electrostatic repulsion between DNA and the residual polymer that is produced from CPCCtat with the caspase-3 cleavage reaction. As a result, caspase-3 signaling should accelerate gene expression.

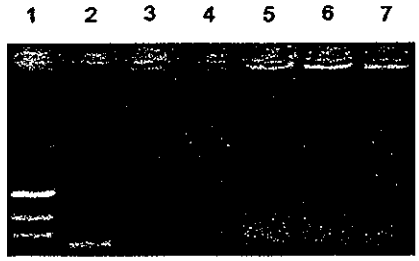

Figure 2. Formation of the CPCCtat–DNA complex and its disintegration with caspase-3 signaling. Lanes 2–4 and 5–7 show the electropherograms of the DNA–CPCCtat complex in the absence and presence of caspase-3, respectively. The ratio of the cationic charge of the CPCCtat (the net charge of each pendant peptide was assumed to be +5) to the phosphate residue in the DNA was 1.0 in lanes 3 and 6, and 2.0 in lanes 4 and 7. Lanes 2 and 5 did not contain the CPCCtat. Lane 1 shows the 1 kb DNA ladder.

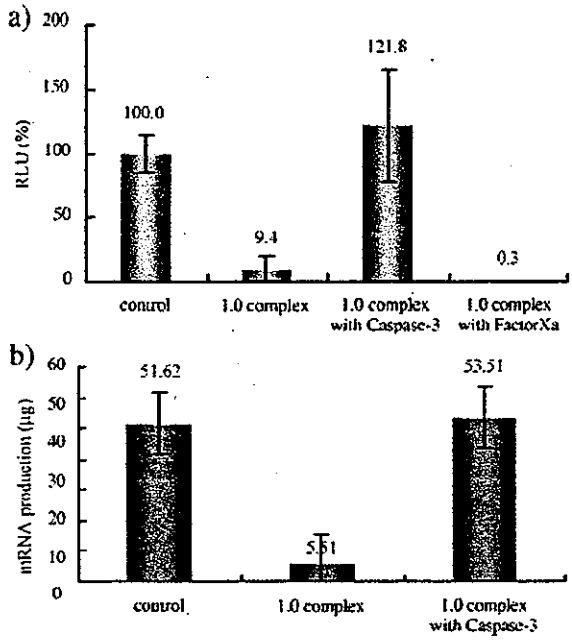

Figure 3. Suppression of luciferase expression with the CPCCtat and its cancellation with caspase-3 signaling in a cell-free system. (a) Luciferase expression in the presence of CPCCtat with or without active caspase-3. (b) Determination of the messenger RNA under the same conditions as in (a).

Effect of Caspase-3 on the Stability of the CPCCtat–DNA Complex and Regulation of Gene Expression in a Cell-Free System. We first investigated whether CPCCtat actually worked as a substrate for caspase-3 using MALDI-TOF mass spectrometry. When the peptide side chain on the CPCCtat is cleaved with caspase-3, the cationic segment of the peptide side chain should be cut off as a fragment peptide (GGRKKRRQRRRPPQ-NH_2, *m/e* = 1775.42). The fragment peptide was detected on the basis of the MS measurement, even in the CPCCtat–DNA complex (data not shown). These results suggest that caspase-3 recognizes the substrate sequence on the side chain in the presence of electrostatic interactions with DNA.

Therefore, the effects of the caspase-3 reaction on the stability of the DNA–CPCCtat complex were investigated using an agarose gel electrophoresis experiment. Addition of the CPCCtat polymer to the DNA solution suppressed the mobility of DNA, indicating the formation of the

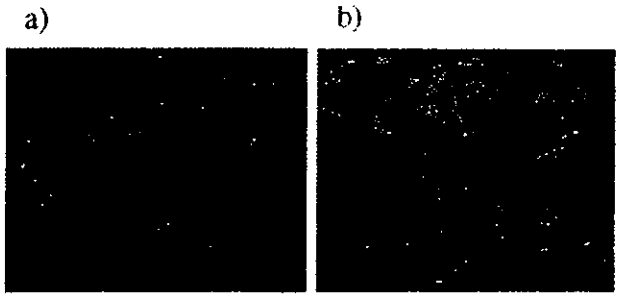

Figure 4. Delivery of the fluorescein-labeled DNA into the NIH 3T3 cell using CPCCtat. (a) Addition of fluorescein-labeled DNA to living cells. (b) Addition of the CPCCtat–fluorescein-labeled DNA complex to living cells.

CPCCtat–DNA complex (Figure 2, lanes 3 and 4). On the other hand, this effect completely disappeared in the presence of active caspase-3 (Figure 2, lanes 6 and 7). This result suggested that the caspase-3 signal could disintegrate the CPCCtat–DNA complex to release the free DNA. Similar polymer–DNA complex formation and disintegration with caspase-3 were observed by atomic force microscopy (data not shown). Figure 3a shows the regulation of gene expression by CPCCtat in a cell-free system. Luciferase expression was significantly suppressed in the formation of the CPCCtat–DNA complex. However, the addition of active caspase-3 to this complex returned the expression ratio to 100% compared with that of free DNA (control). In contrast, when we used another protease, factor Xa, gene expression did not recover. The messenger RNA levels were also determined in each experiment. The mRNA levels in the presence of CPCCtat or after treatment with caspase-3 corresponded to the gene expression levels under the same conditions (Figure 3b). These results indicate that CPCCtat can regulate gene expression in its transcription step on the basis of the change of the carrier–DNA complex stability, and that its activation is selective in response to the caspase-3 signal.

Gene Delivery Using CPCCtat and the Apoptotic Cell-Specific Gene Expression of the Delivered Gene in Cultured Cells. All the results mentioned above were very similar to those obtained in our previous research using a similar polymer–peptide conjugate (CPCC), which had oligolysine instead of a Tat peptide as the cationic portion. However, our previous polymer (CPCC) could not deliver any genes into living cells. Therefore, in the present study we applied the CPCCtat system to gene delivery into cells because CPCCtat possesses as its cationic region the Tat peptide, which is a cellular membrane-permeable peptide, a so-called PTD (protein transduction domain). In fact, the complex derived from CPCCtat and fluorescein-labeled DNA (1234 bp) at a charge ratio of 1 was successfully delivered into NIH 3T3 cells on the basis of fluorescence microscope observations (Figure 4). This improvement in transfection efficiency depends on the existence of the Tat peptide, which facilitates the internalization of the CPCCtat–DNA complex in a nonendocytotic manner. After the gene was delivered using CPCCtat, regulation of gene expression in response to intracellular caspase-3 was possible. When a GFP-encoding plasmid was delivered with the CPCCtat for 15 min at 37 °C, no fluorescence was observed in any cells after 24 h, meaning that gene expression was totally suppressed. In contrast, when a GFP-encoding plasmid was delivered into the caspase-3-activated cells, which was stimulated by staurosporine, weak fluorescence derived from GFP was observed in the cytosol after 4 h of delivery (data not shown). However, this fluorescence intensity was so weak that more sensitivity was necessary to evaluate the extent of gene expression quantitatively responding to the intracellular caspase-3 signaling, probably due to the poor efficiency of gene delivery into the cells. We therefore tried to increase the amount of CPCCtat–DNA complex incorporated into living cells using HVJ-E. HVJ-E is an inactivated virus envelope, and it can deliver a gene inside its

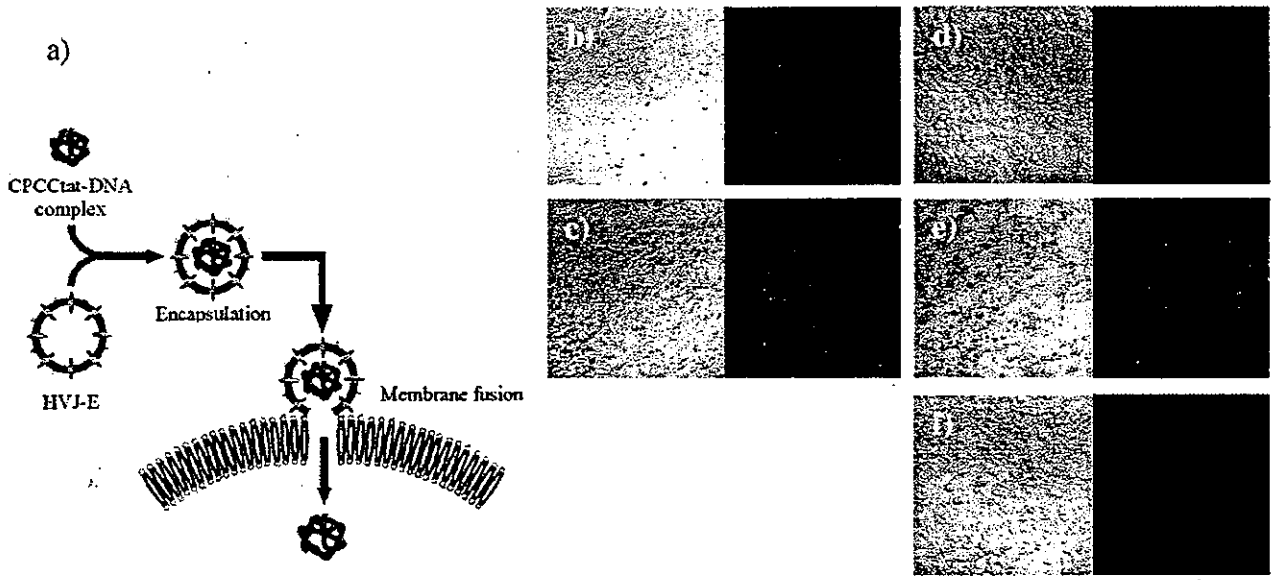

Figure 5. Delivery of the CPCCtat–DNA complex to NIH 3T3 cells with HVJ-E and apoptotic cell-selective expression of GFP. (a) Scheme of the CPCCtat–DNA complex delivery into cells with HVJ-E. (b–f) GFP-encoding DNA–CPCCtat complexes at a charge ratio of 1.0 and 2.0 were encapsulated by HVJ-E and delivered into NIH 3T3 cells without apoptotic stimulation (b and d), or 15 h after apoptotic stimulation (c and e). (f) Same experiment as (e) using $CPCC_{EVEE}$ instead of CPCCtat. One hour after the addition of the HVJ-E-encapsulating CPCCtat–DNA complex, the cells were treated with staurosporin as the apoptotic stimulant (c, e, f).

envelope through membrane fusion between HVJ-E and the target cell.[22] We applied HVJ-E to encapsulate the CPCCtat–DNA complex. The HVJ-E-encapsulating CPCCtat–DNA complex was taken up by the cultured cells through membrane fusion, and the polymer–DNA complex inside the HVJ-E was effectively delivered into the cells (Figure 5a). The CPCCtat–DNA (GFP-encoding) complex at a charge ratio of 1 or 2 (+/−) was successfully incorporated into HVJ-E. Then, the HVJ-E encapsulating the CPCCtat–DNA complex was added to the NIH 3T3 cells. When the complex at a charge ratio of 1 was delivered into the cells, weak fluorescence derived from GFP was observed after 16 h of delivery (Figure 5b), even in normal cells without apoptotic stimulation. On the other hand, the expression of GFP was completely suppressed in normal cells in the case of a charge ratio of 2 (Figure 5d). These results probably indicate that the increase in cationic polymer levels more effectively augments the steric hindrance of the acrylamide main chain in CPCCtat to prevent the access of RNA polymerase to DNA in the case of a charge ratio of 2. We monitored the fluorescence in the cellular sample for 2 days after addition of the complex, but any gene expression did not appear. This suppression of gene expression cannot be applied with similar efficiency to ordinary cationic polymers such as poly-L-lysine or its derivatives. In fact, poly-L-lysine cannot suppress luciferase expression under the same conditions as those shown in Figure 3a.

CPCCtat activated GFP expression only in the case of caspase-3 activation (Figure 5c,e). After 15 h of stimulation with staurosporine (1 μM), fluorescence derived from GFP was observed in complex-delivered cells with charge ratios of both 1 and 2. We estimated the intracellular activity of caspase-3 using a fluorescent substrate of caspase-3. (Ac-DEVD-NH-coumarin) by monitoring the fluorescence intensity at 490 nm (data not shown). In this case, the activity of the intracellular caspase-3 was around 2 U after 2–3 h of the staurosporine treatment. This activity was similar to that which we used in the cell-free experiment. Thus, it was reasonable that this activation of the gene expression was caused by the intracellular caspase-3. Additionally, we examined the same experiment with the control polymer $CPCC_{EVEE}$, in which the substrate sequence of DEVD was changed to EVEE. This sequence does not work as the substrate of caspase-3, but it has the same anionic charge as DEVD. Figure 5f shows the results of the GFP expression assay with $CPCC_{EVEE}$ using NIH 3T3 cells. Under these conditions, no fluorescence was observed, even if the caspase-3 was activated with staurosporine. These results indicate that CPCCtat can actually regulate the delivered gene expression in the living cells specifically responding to the intracellular caspase-3 signaling. We are now trying to rescue target cells from apoptosis, using the apoptosis inhibitor-encoding gene with the CPCCtat system.

Conclusion

We report here a new class of gene carrier based on the D-RECS system. The CPCCtat polymer can activate the delivered gene expression responding to target intracellular signaling (caspase-3 activity). This system should advance the development of cell-specific gene therapy, since the occurrence of unusual intracellular signaling is essential in almost all diseases. Our strategy therefore has the potential to be applied to various diseases. In fact, we have previously reported another type of polymer–peptide conjugate responding to protein kinase A signaling. This polymer regulates gene expression in a cell-free system very similarly to the CPCCtat polymer. Such systems will offer a new approach to the design of a cell-specific gene expression system.

Acknowledgment. This work was financially supported by CREST, the Japan Science Corp., a grant-in-aid for Scientific Research from the Ministry of Education, Science, Sports, and Culture in Japan, and a grant-in-aid for Scientific Research from the Ministry of Health, Labour and Welfare.

References and Notes

(1) http://www.wiley.co.uk/wileychi/genmed/clinical/.
(2) Varga, C. M.; Wickham, T. J.; Lauffenburger, D. A. Receptor-Mediated Targeting of Gene Dlivery Vectors: Insights from Molecular Mechanisms for Improved Vehicle Design. *Biotechnol. Bioeng.* **2000**, *70*, 593–605.
(3) Hood, J. D.; Bednarski, M.; Frausto, R.; Guccione, S.; Reisfeld, R. A.; Xiang, R.; Cheresh, D. A. Tumor Regression by Targeted Gene Delivery to the Neovasculature. *Science* **2002**, *296*, 2404–2407.
(4) Meers, P. Enzyme-activated targeting of liposomes. *Adv. Drug Delivery Rev.* **2001**, *53*, 265–272.
(5) Torchilin, V. P. Drug targeting. *Eur. J. Pharm. Sci.* **2000**, *11*, S81–S91.
(6) Garnett, M. C. Targeted drug conjugates: principles and progress. *Adv. Drug Delivery Rev.* **2001**, *53*, 171–216.
(7) Kato, Y.; Onishi, H.; Machida, Y. Biological characteristics of lactosaminated N-succinyl-chitosan as a liver-specific drug carrier in mice. *J. Controlled Release* **2001**, *70*, 295–307.
(8) Hartmann, A.; Hunot, S.; Michel, P. P.; Muriel, M. P.; Vyas, S.; Faucheux, B. A.; Mouatt-Prigent, A.; Turmel, H.; Srinivasa, A.; Ruberg, M.; Evan, G. I.; Agid, Y.; Hirsch, E. C. Caspase-3: A vulnerability factor and final effector in apoptotic death of dopaminergic neurons in Parkinson's disease. *Proc. Natl. Acad. Sci. U.S.A.* **2000**, *97*, 2875–2880.
(9) Gopalakrishna, R.; Jaken, S. Protein kinase C signaling and oxidative stress. *Free Radical Biol. Med.* **2000**, *28*, 1349–1361.
(10) Graff, J. R.; Konicek, B. W.; McNulty, A. M.; Wang, Z.; Houck, K.; et al. Increased AKT activity contributes to prostate cancer progression by dramatically accelerating prostate tumor growth and diminishing p27Kip1 expression. *J. Biol. Chem.* **2000**, *275*, 24500–24505.
(11) Page, C.; Huang, M.; Jin, X.; Cho, K.; Lilja, J.; Reynolds, R. K.; Lin, J. Elevated phosphorylation of AKT and Stat3 in prostate, breast, and cervical cancer cells. *Int. J. Oncol.* **2000**, *17*, 23–28.
(12) Kim, S. H.; Forman, A. P.; Mathews, M. B.; Gunnery, S. Human breast cancer cells contain elevated levels and activity of the protein kinase, PKR. *Oncogene* **2000**, *19*, 3086–3094.
(13) Price, D. T.; Rocca, G. D.; Guo, C.; Ballo, M. S.; Schwinn, D. A.; Luttrell, L. M. Activation of extracellular signal-regulated kinase in human prostate cancer. *J. Urol.* **1999**, *162*, 1537–1542.
(14) Nemoto, T.; Ohashi, K.; Akashi, T.; Johnson, J. D.; Hirokawa, K. Overexpression of protein tyrosine kinases in human esophageal cancer. *Pathobiology* **1997**, *65*, 195–203.
(15) Shimizu, T.; Usuda, N.; Sugenoya, A.; Masuda, H.; Hagiwara, M.; Hidaka, H. Immunohistochemical evidence for the overexpression of protein kinase C in proliferative diseases of human thyroid. *Cell. Mol. Biol.* **1991**, *37*, 813–821.
(16) Katayama, Y.; Sonoda, T.; Maeda, M. A Polymer Micelle Responding to the Protein Kinase A Signal. *Macromolecules* **2001**, *34*, 8569–8573.
(17) Katayama, Y.; Fujii, K.; Ito, E.; Sakakihara, S.; Sonoda, T.; Murata, M.; Maeda, M. Intracellular Signal-Responsive Artificial Gene

Regulation for Novel Gene Delivery. *Biomacromolecules* 2002, *3*, 905−909.
(18) Sakakihara, S.; Fujii, K.; Katayama, Y.; Maeda, M. A novel regulation system of gene expression responding to protease signal. *Nucleic Acids Res.* 2001, Suppl. 1, 149−150.
(19) Cohen, G. M. Caspases: the executioners of apoptosis. *Biochem. J.* 1997, *326*, 1−16.
(20) Lindgren, M.; Hällbrink, M.; Prochiantz, A.; Langel, Ü. Cell-penetrating peptides. *Trends Pharmacol. Sci.* 2000, *21*, 99−103.
(21) Schwarze, S. R.; Hruska, K. A.; Dowdy, S. F. Protein transduction: unrestricted delivery into all cells? *Trends Cell Biol.* 2000, *10*, 290−295.
(22) Kaneda, Y.; Nakajima, T.; Nishikawa, T.; Yamamoto, S.; Ikegami, H.; Suzuki, N.; Nakamura, N.; Morishita, R.; Kotani, H. Hemagglutinating virus of Japan (HVJ) envelope vector as a versatile gene delivery system. *Mol. Ther.* 2003, *6*, 219−226.

BM0493887

Available online at www.sciencedirect.com
SCIENCE DIRECT
Bioorganic & Medicinal Chemistry Letters
ELSEVIER
Bioorganic & Medicinal Chemistry Letters 14 (2004) 847–850

Mass-tag technology for monitoring of protein kinase activity using mass spectrometry

Tatsuhiko Sonoda,[a] Syuhei Shigaki,[a] Takeyuki Nagashima,[b] Osamu Okitsu,[b] Yasuhiro Kita,[b] Masaharu Murata[a] and Yoshiki Katayama[a,*]

[a]*Department of Applied Chemistry, Graduate School of Engineering, Kyushu University, Hakozaki, Higashi-ku, Fukuoka 812-8581, Japan*
[b]*Advanced Technology Platform Laboratory, Fujisawa Pharmaceutical Co. Ltd, 2-3 Tokodai, Tsukuba 300-2698, Japan*

Received 7 October 2003; revised 27 November 2003; accepted 4 December 2003

Abstract—Monitoring of intracellular protein kinase activity is very important for fields involving diagnosis and drug screening. However, current methods, such as radiometry using ^{32}P, or ELISA, are laborious and time-consuming. We have developed high-throughput assay system of protein kinase activity using mass-tagged substrate peptide probes and mass spectrometry. This assay system can easily evaluate target kinase activity and will potentially be able to simultaneously profile many protein kinase activities.

Cells possess an intracellular signal transduction system with which they can precisely respond to their outer environment. The system consists of many chemical reaction cascades, and many proteins are associated with these reactions. Intracellular signals are primarily transduced by protein activation (or inactivation) caused by the conformation changes in proteins. Protein phosphorylation is one of the most versatile reactions in cells that can cause protein-conformational change. This reaction is catalyzed by protein kinases and controls various cellular functions, including gene expression,[1] cellular proliferation,[2] and cell death.[3] Therefore, if the enzymatic activity of a protein kinase rises abnormally, this rise can be directly related to various diseases.[4–6] It will therefore be useful to develop an assay system for protein kinases activities in cellular samples for fields involving diagnosis, evaluation of gene-functions, and drug development. Radiometry[7] using ^{32}P, or ELISA[8–10] well known as such an assay system. Although these assays are quite sensitive, they are laborious and time-consuming. Therefore, the development of high-throughput assay systems is required to profile all the protein kinase activity of many samples.

We report herein the use of a mass-tag strategy in an assay system for protein kinase activity using mass spectrometry. Figure 1(a) shows the basic concept of this detection system. Two cellular samples representing two different states are homogenated, respectively, and two types of peptide probes are separately added to each cell lysate. These probes possess the same substrate peptide sequences for the target protein kinase, while one of these peptide probes is isotopically heavier than the other due to the incorporation of deuterium into acetyl groups in the peptide probe. Therefore, two peptides can be distinguished in the mass spectrum. The *m/z* values of these probes increase by +80 with phosphorylation by the target protein kinase, so that protein kinase activities between different cellular states can be compared directly by calculating the phosphorylated ratio in each probe using the peak intensity in the mass spectrum after the both probe solutions were combined.

According to this concept, the peptide probes, PKA-H_6 and PKA-D_6, which possessed the substrate sequence of protein kinase A (PKA) and the His-Tag sequence, R_2-KHHHHHHGLRRASLKC-NH_2 (R = CH_3CO– or CD_3CO–), were designed and synthesized. In these probes, two normal acetyl groups or deuterated acetyl groups were incorporated into the lysine residue at the amino-terminus. Thus, the difference between the mass numbers of these probes is 6. We chose protein kinase A

Keywords: Protein kinases; Protein phosphorylation; High-throughput screening; Mass spectrometry.
* Corresponding author. Tel.: +81-926-424-206; fax: +81-926-423-606; e-mail: ykatatcm@mbox.nc.kyushu-u.ac.jp

0960-894X/$ - see front matter © 2003 Elsevier Ltd. All rights reserved.
doi:10.1016/j.bmcl.2003.12.022

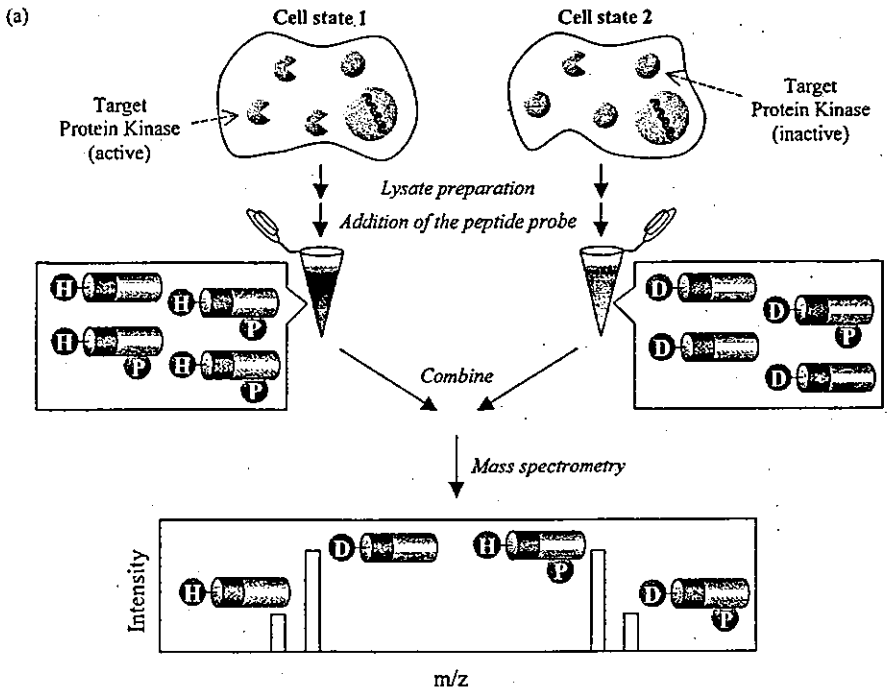

Figure 1. (a) Schematic outline of the protein kinase activity assay system using mass spectrometry. (b) Amino acid sequences of PKA substrate peptide probes.

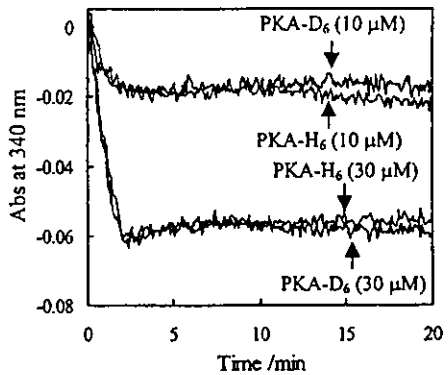

Figure 2. The time-dependent decrease in the absorbance at 340 nm based on the oxidation of NADH, which was led by the phosphorylation of the peptide probes by PKA in the coupled enzyme assay. The experiment was performed with 10 or 30 μM of each peptide probe in PBS(−) (pH 7.2) containing 0.2 mM ATP, 10 mM $MgCl_2$, 1 mM phosphoenolpyruvate, 0.3 mM NADH, 12 units of lactate dehydrogenase, 4 units of pyruvate kinase, and 60 units of PKA C-subunit at 24 °C.

(PKA) as the first target protein kinase because the enzyme is one of the most important protein kinases and controls many cellular functions such as gene expression,[11] hormone secretion,[12] and cell differentiation.[13] Meanwhile, the His-Tag sequence was introduced in peptide probes to purify them from the cell lysate in case pre-purification of the probes was required. Acetylated peptide probes were synthesized with automatic peptide synthesizer by Fmoc chemistry using corresponding Fmoc-amino acids and Fmoc-Lys(Fmoc)-OH as the N-terminal amino acid [Fig. 1(b)]. In the case of deuterated peptide synthesis, acetic anhydride-d_6 was used as the N-terminal acetylation reagent.

We first investigated whether deuterium labeling of the peptide influenced the kinetics of phosphorylation with PKA. The phosphorylation of these probes was monitored spectrophotometrically with a coupled enzyme assay reported by Cook et al.[14] In this assay, the production of ADP, which is derived from ATP as a byproduct of the phosphorylation, finally brings about an oxidation of NADH using pyruvate kinase and lactate dehydrogenase. The phosphorylation can therefore be monitored as the decrease in absorbance at 340 nm. As shown in Figure 2, the profile of the absorbance-decrease accompanying phosphorylation of the heavy probe (PKA-D_6) showed good agreement with that of the light probe (PKA-H_6), meaning that neither of the peptides differed in their ability to function as a substrate to PKA.

For the next experiment, we examined whether the mass spectra arising from both the peptide probes could be differentiated from each other. Phosphorylated or non-phosphorylated peptide probe solution was prepared separately and mixed together, then analyzed by MALDI-TOF MS. As a result, four peaks were distinctly observed. The following experiment was then performed to confirm that the phosphorylation processes of the peptide probes could be monitored by mass spectrometry. Two sample solutions of PBS(−) containing 4 U/mL PKA, 0.2 mM ATP, and 10 mM $MgCl_2$ were prepared. PKA-H_6 and PKA-D_6 were added separately to each sample to a final concentration of 2

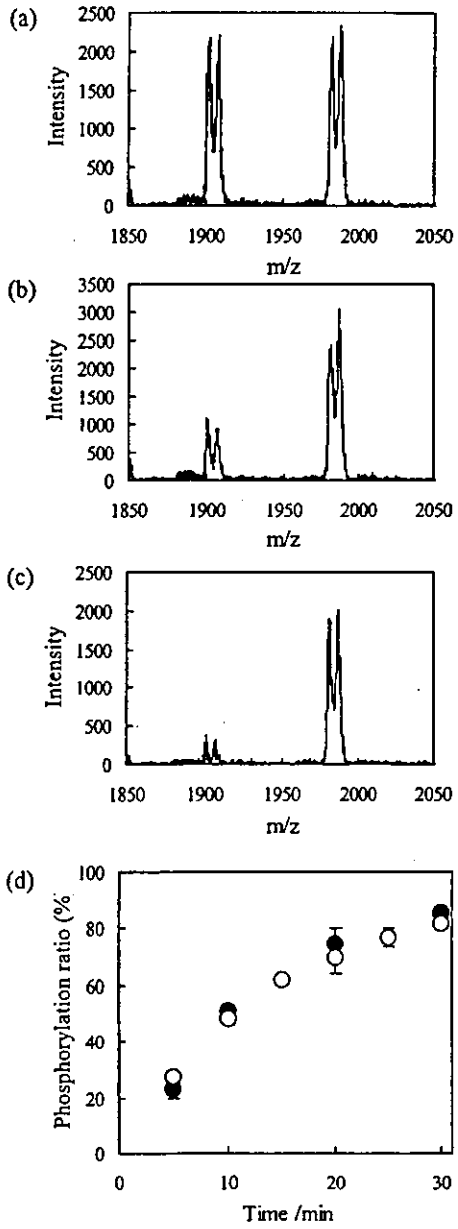

Figure 3. Mass spectra (a) 10 min, (b) 20 min, and (c) 30 min after adding the PKA C-subunit. (d) The time-dependent increase in the phosphorylation ratio calculated from the intensities of the mass peaks (open ciecle: PKA-H_6, closed circle: PKA-D_6).

μM, and the sample was then incubated at 37 °C. Next, 1 μL of each probe solution was taken in every 5 min after addition of the peptide probe, and the two solutions were combined, followed by analysis with MALDI-TOF MS. Figure 3 shows the typical mass spectra and time-dependence of the phosphorylation ratio calculated from the intensities of these mass peaks. The intensities of the mass peaks arising from nonphosphorylated probes (*m/z*: 1900.99 for PKA-H_6 and 1906.03 for PKA-D_6) gradually decreased with the reaction time, and those from phosphorylated probes (*m/z*: 1980.43 and 1986.44 for PKA-H_6 and PKA-D_6, respectively) increased at the same time. The time course of the phosphorylations showed good coincidence in the

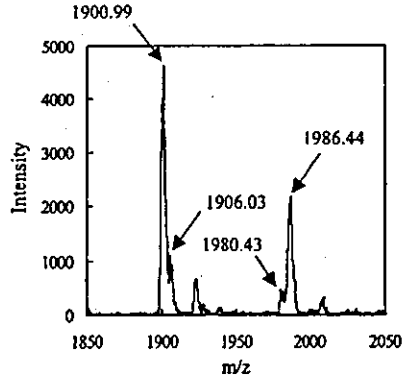

Figure 4. The mass spectrum from the mixture of two samples that contained different PKA activities. The concentration of PKA in PKA-H6 and PKA-D6 solutions were 30 U and 6 U, respectively. Each solution was combined to measure MALDI-TOF MS, after 3 h incubation at 37 °C.

two probes. These results suggested that the phosphorylation processes with PKA could be evaluated by the assay system using mass spectrometry.

For the last experiment, we investigated whether the difference in the PKA activities of the two samples, which contained different amounts of activated PKA, could be evaluated using this assay system. Thus, PKA-H_6 or PKA-D_6 (each 100 μM at a final concentration) was added to the PBS(−) containing 0.2 mM ATP and 10 mM $MgCl_2$ and activated PKA. The PKA activity in each probe solution was 6 U/mL and 30 U/mL for PKA-H_6 and PKA-D_6, respectively. After incubating for 3 h at 37 °C, these solutions were combined and analyzed by MALDI-TOF MS. The obtained mass spectrum (Fig. 4) shows that PKA-D_6, which was added to the sample with higher PKA activity, was more phosphorylated than the PKA-H_6. The peak height of the nonphosphorylated PKA-H_6 was nearly 5 times higher than that of nonphosphorylated PKA-D_6. On the other hand, the peak height of phosphorylated PKA-D_6 was approximately 5 times higher. These results reflect the differences in PKA activity between the two sample solutions quite well. Thus, this assay system was found to be potentially useful for evaluating PKA activity.

We are now attempting to apply this system to the measurement of PKA activity in cellar lysates. Moreover, the mass-tag strategy reported here can easily be applied to the probe peptides for monitoring other protein kinase activities. In this assay system, dozens of peptide probes can be detected simultaneously if each probe is designed to have a distinct mass number. As such, this system will potentially be able to simultaneously profile many protein kinase activities.

Acknowledgements

This work was supported by a grant-in-aid from the New Energy and Industrial Technology Development Organization (NEDO) and also by Regional Science Promotion Program, JST Co.

References and notes

1. Treisman, R. *Curr. Opin. Cell Biol.* **1996**, *8*, 205.
2. Kato, Y.; Tapping, R. I.; Huang, S.; Watoson, M. H.; Ulevitch, R. J.; Lee, J. D. *Nature* **1998**, *395*, 713.
3. Hartmann, A.; Hunot, S.; Michel, P. P.; Muriel, M. P.; Vyas, S.; Faucheux, B. A.; Mouatt-Prigent, A.; Turmel, H.; Srinivasa, A.; Ruberg, M.; Evan, G. I.; Agid, Y.; Hirsch, E. C. *Proc. Natl. Acad. Sci. U.S.A.* **2000**, *97*, 2875.
4. Kim, S. H.; Forman, A. P.; Mathews, M. B.; Gunnery, S. *Oncogene* **2000**, *19*, 3086.
5. Nabel, G. J.; Nabel, E. G.; Yang, Z. Y.; Fox, B. A.; Plautz, G. E.; Gao, X.; Huang, L.; Shu, S.; Gordon, D.; Chang, A. E. *Proc. Natl. Acad. Sci. U.S.A.* **1993**, *90*, 11307.
6. Page, C.; Huang, M.; Jin, X.; Cho, K.; Lilja, J.; Reynolds, R. K.; Lin, J. *J. Oncol.* **2000**, *17*, 23.
7. Chinery, R.; Brockman, J. A.; Dransfield, D. T.; Coffey, R. J. *J. Biol. Chem.* **1997**, *272*, 30356.
8. Tamaskovic, R.; Forrer, P.; Jaussi, R. *Biol. Chem.* **1999**, *380*, 569.
9. Lehel, C.; Daniel-Issakani, S.; Brasseur, M.; Strulovici, B. *Anal. Biochem.* **1997**, *244*, 340.
10. Ross, H.; Armstrong, C. G.; Cohen, P. *Biochem. J.* **2002**, *366*, 977.
11. Montminy, M. *Annu. Rev. Biochem.* **1997**, *66*, 807.
12. McCusker, R. H.; Clemmons, D. R. *J. Cell. Physiol.* **1998**, *174*, 293.
13. Bertolotto, C.; Abbe, P.; Hemesath, T. J.; Bille, K.; Ficher, D. E.; Ortonne, J. P.; Ballotti, R. J. *J. Cell Biol.* **1998**, *142*, 827.
14. Cook, P. F.; Neville, M. E.; Vrana, K. E.; Hartl, F. T.; Roskoski, R. *Biochemistry* **1982**, *21*, 5794.

ANALYTICAL SCIENCES JANUARY 2004, VOL. 20

Rapid Communications

First Functionalized MRI Contrast Agent Recognizing Vascular Lesions

Tatsuhiro YAMAMOTO,*1 Kenjiro IKUTA,*1 Keiji OI,*2 Kohtaro ABE,*2 Toyokazu UWATOKU,*2 Masaharu MURATA,*1 Noboru SHIGETANI,*3 Kengo YOSHIMITSU,*4 Hiroaki SHIMOKAWA,*2 and Yoshiki KATAYAMA*1†

*1 *Department of Applied Chemistry, Faculty of Engineering, Kyushu University, Fukuoka 812-8581, Japan*
*2 *Department of Cardiovascular Medicine, Kyushu University Graduate School of Medical Sciences, Fukuoka 812-8582, Japan*
*3 *Department of Radiology, Kyushu University Hospital, Fukuoka 812-8582, Japan*
*4 *Department of Clinical Radiology, Graduate School of Medical Sciences, Kyushu University, Fukuoka 812-8582, Japan*

A new MRI-contrast agent, EB-DTPA-Gd, that has an Evans Blue analogue as a sensing unit for endothelium lesions, was designed and synthesized. The agent also has diethylenetriamine-*N,N,N',N'',N''*-pentaacetic acid-Gd complex (Gadolinium-DTPA) units, which have been used as detection units for T1-weighted MRI. The EB-DTPA-Gd was able to recognize and adsorb to the vascular endothelium-denuded region of porcine aorta, and to decrease the relaxation time of circumferential water's protons, making possible MR imaging of the endothelium-denuded region. The compound can be employed as a contrast agent for the imaging of vascular lesions using MRI.

(Received November 6, 2003; Accepted November 26, 2003)

Vascular endothelium plays a very important role in regulating vascular homeostasis. If the endothelium is damaged, this vascular lesion often leads to a cardiovascular disease, such as arteriosclerosis or spasms in the coronary artery.[1] Therefore, the detection and evaluation of vascular endothelium lesions in their early stage would be very important for effective diagnosis and therapy. However, no practical method for vascular lesion-specific detection has been reported as a practical diagnostic tool.

In this report, we describe a novel endothelium lesion-specific MRI (Magnetic Resonance Imaging) contrast agent, which has a dye component as a probing unit for the vascular lesion. In general, biomolecules such as antibodies, polysaccharides, or peptides have been used to recognize particular sites in biological systems.[2-4] However, such biomolecules are very expensive and are thus not practical for a contrast agent for blood vessels due to the large blood flow, in which a large amount of the agent would be needed. Therefore, we have looked for other less-expensive molecules that can recognize vascular endothelium lesions using the porcine aorta, and have at last found certain types of organic dyes to be useful for this purpose. In histochemistry, various dyes have been used for staining specific tissues and proteins.[5-7] These dyes can interact with their targets with high specificity. For example, Congo Red specifically binds to the amyloid beta protein.[7] In these dyes, Evans Blue has been used for staining a vascular endothelium injury.[8] Vascular endothelium forms a tight junction that regulates the molecular permeability into the vascular wall from the blood,[9] thereby providing a barrier in the vascular wall against blood flow. If the vascular endothelium is injured, many molecules begin to interact with the extracellular matrix and the vascular smooth muscle layer, which is located below the endothelium layer.

We have recently synthesized structural analogues of Evans Blue, and the dye unit was observed to selectively adsorb to a vascular endothelium-denuded region. We have therefore designed a new MRI-contrast agent that has Evans Blue analogue (Fig. 1). The compound can be used as a contrast agent for the imaging of vascular lesions using MRI.

Experimental

Synthesis of N-tert.butoxycarbonyl-2,2'-dimethylbenzidine

2,2'-Dimethylbenzidine (3.00 g, 14.1 mmol) was dissolved in dichloromethane (25 ml), and Boc-anhydride (3.08 g, 14.1 mmol) was added dropwise at r.t. while stirring. After overnight stirring, the remaining dimethylbenzidine was removed by washing with saturated aqueous tartaric acid. The organic phase was then concentrated under reduced pressure. The residue was purified by column chromatography on silica gel using ethylacetate-hexane (3:5) as an eluting solvent. The

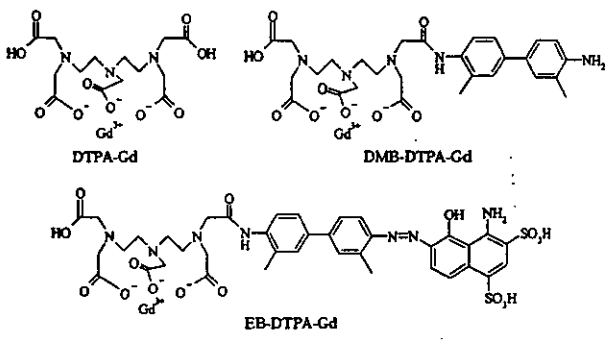

Fig. 1 Chemical structure of the MRI contrast agent.

† To whom correspondence should be addressed.

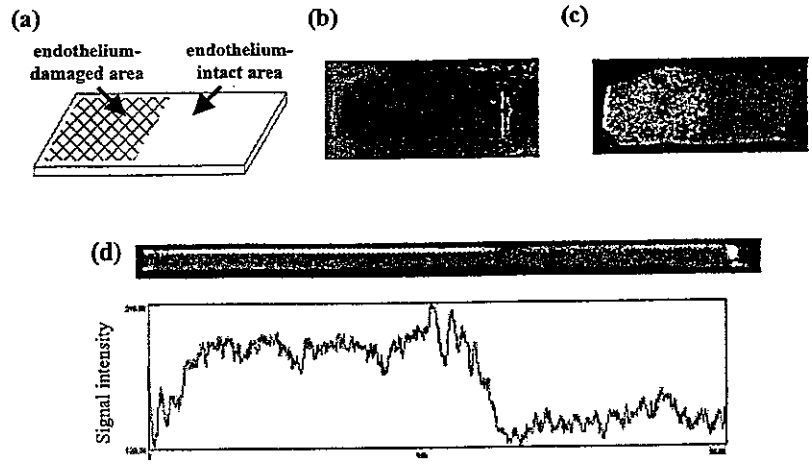

Fig. 2 MR imaging result of an opened porcine aorta strip stained with 10 mM aqueous EB-DTPA-Gd solution. (a) Schematic illustration of the blood vessel sample. (b) Photograph of the blood vessel stained with EB-DTPA-Gd. (c) and (d) MR images of the surface of the inner wall and the cross section of the blood vessel sample, respectively, of the sample (TR/TE = 400/14 ms). The signal intensity profile is also shown in (d).

desired product was obtained as a pale-yellow solid (1.91 g, 43%). The chemical structure was determined with ^{1}H-NMR and elemental analysis.

Synthesis of 2,2′-dimethylbenzidine-DTPA (DMB-DTPA)

N-tert.butoxycarbonyl-2,2′-dimethylbenzidine (0.281 g, 0.899 mmol) and DTPA anhydride (0.481 g, 1.35 mmol) were dissolved in dry DMSO (15 ml). The mixture was stirred at 40°C. After 3 h, the reaction mixture was poured into cold water (500 ml). The precipitate was collected by filtration. The collected solid was put into water (2.8 ml), and the pH of the suspension was then adjusted to 7 with sodium carbonate. After neutralization, the solid was dissolved completely and then purified by ODS column chromatography using water-acetonitrile (3:1). The desired fraction was collected and then freeze-dried. The obtained solid was redissolved in TFA (5 ml), followed by stirring at r.t. for 1 h. This solution was poured into cold ether. The deposited solid was collected by filtration and dried under reduced pressure to obtain a colorless solid (0.133 g, 14%). The chemical structure was characterized as TFA salts (DMB-DTPA·4TFA) by ^{1}H-NMR and elemental analysis.

Synthesis of EB-DTPA

All reactions were performed in an ice bath. DMB-DTPA·4TFA (51.1 mg, 49.0 mmol) was dissolved in water (1 ml) containing HCl (147 μmol). Sodium nitrite (3.38 mg, 49.0 μmol) was then added in small portions, followed by stirring for 20 min. A diazonium salt solution was added dropwise into 1 ml of an aqueous 1-amino-8-naphtol-2,4-disulfonic acid (16.7 mg, 49.9 μmol) solution containing sodium bicarbonate (16.5 mg, 196 μmol), and then stirred for 3 h. The reaction mixture was lyophilized. The concentrate was redissolved in water (1 ml), and the desired product was precipitated by conc. hydrochloric acid (36.5 mg, 81%). The precipitate was collected and dried under reduced pressure. The chemical structure was determined by ^{1}H-NMR and elemental analysis.

MRI experimental procedure

An aqueous MRI contrast agent solution was prepared as follows. EB-DTPA was dissolved in deionized water to be 1 - 15 mM, and a 1 M aqueous gadolinium chloride solution containing equimolar gadolinium ion to EB-DTPA was added. The pH of the solution was adjusted to 7 with a 1 M aqueous sodium hydroxide solution.

An extracted porcine aorta was opened to a flat sheet. The endothelium in the left-half area from the center axis was then removed with a scalpel, while the right-half area was allowed to remain intact (Fig. 2a). The aorta section was dipped with the MRI contrast agent solution for 10 s, and then washed with saline. The aorta section was evaluated by MR Imaging (1.5T MAGNETOM VISION system (SIEMENS, Germany), T1-weighted Spin Echo, TR/TE=400/14 ms, 3 mm slice thickness, field-of-view 50 mm and dot matrix 128*256). The obtained MRI image was analyzed with the NIH image.

Results and Discussion

The MRI contrast agent was successfully obtained as a pure compound by the preparation protocol described in the experimental section. We therefore investigated whether the molecule selectively bound to an endothelium-broken site in a blood-vessel sample.

A photograph of the porcine aorta stained with 10 mM aqueous MRI contrast agent, EB-DTPA-Gd, is shown in Fig. 2b. Although a slight nonspecific binding of the agent was observed in the intact endothelium region, a clear accumulation of the synthesized contrast agent was observed in the endothelium-removed region. Figure 2c shows an MRI image, giving a top view. The endothelium-intact area and the damaged area can be distinguished by T1-weighted MR imaging. Figure 2d shows an MRI image of the same aorta section, but a side view, and a histogram of the MR signal intensity on the inner-surface region of the aorta section. The stained section shows that the MRI signal enhancement can only be seen in the inner-surface area of the aorta wall, which means that EB-DTPA-Gd did not permeate the tissue from the endothelium barrier-injured site. This result is quite important because the MR imaging agent for blood vessels should be excreted rapidly after the MR image is taken; otherwise, an undesired effect might result. In the localization of the agent at the surface area, the polar group in the Evans Blue-related structure may be requisite. Actually, the MR-signal using DMB-DTPA-Gd, which lacked the 2,4-disulfonyl-1-amino-8-naphtol unit from EB-DTPA-Gd, was seen even in the smooth

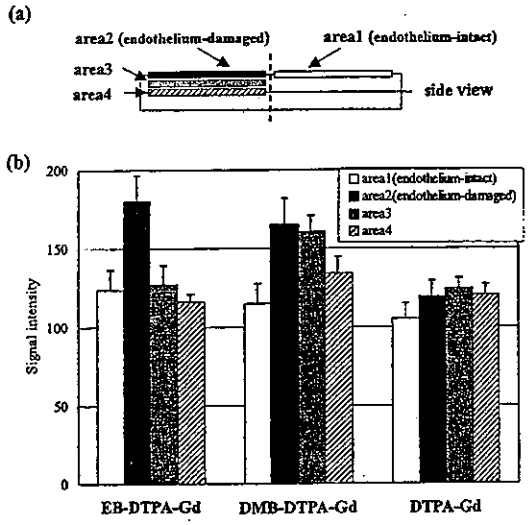

Fig. 3 Structural effects of the tissue absorption in the DTPA-type MRI contrast agents (10 mM). (a) Schematic illustration of the aorta section in the side view. (b) MRI signal was measured from four areas indicated by area 1 - 4 in the figure, separately. The error bars represent the standard deviation.

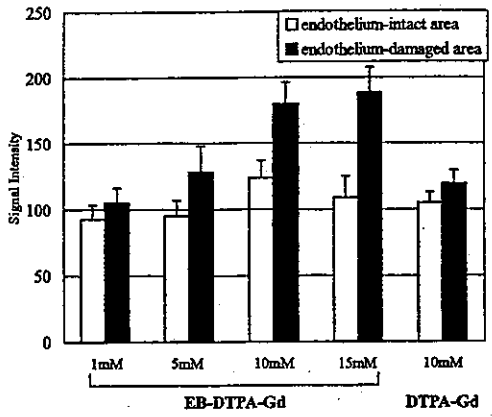

Fig. 4 Dose dependence of the MRI-signal in the endothelium lesion and the intact region using EB-DTPA-Gd or DTPA-Gd. The error bars represent the standard deviation.

muscle layer of the aorta strip due to infiltration of the compound (Fig. 3b). In contrast, an ordinary MRI-contrast agent, DTPA-Gd, which had no hydrophobic unit, did not adsorb on the inner surface of the aorta sample. These results indicate that the endothelium lesion-selective contrast agent should have a chemical structure that is hydrophobic, but that at the same time has some hydrophilic groups.

For the next experiment, the concentration dependency of the MRI signal of the EB-DTPA-Gd of endothelium lesion was evaluated to determine the minimal dose. First, the contrast agent was evaluated (Fig. 4). The MRI signal intensity was gradually increased in the endothelium-damaged area along with increases in the EB-DTPA-Gd concentrations. In contrast, the MRI signals of the endothelium-intact area were found to be independent of the agent concentrations. The increment of the signal intensity was nearly saturated at agent concentrations of 10 mM on the lesional area. Thus, we determined that 10 mM is sufficient to detect the target area. The signal increment when using of 10 mM EB-DTPA-Gd was nearly 1.5-times that of the intact area.

Endothelium lesions often cause vascular diseases. For the diagnosis of such an endothelium-damaged site, we tried to design an MRI-contrast agent that can bind to such a vascular injury site.

After a wide range of screening, we finally found some organic azo-dyes that could potentially be used as a probing unit for endothelium lesions, and Evans Blue was found to be the best candidate among these dyes. Thus, we designed a new MRI contrast agent, EB-DTPA-Gd, having an Evans Blue-related structure. Newly synthesized EB-DTPA-Gd showed endothelium lesion-specific adsorption in an *in vitro* experiment. The reagent was also able to detect the lesional site using T1-weighted MR-imaging. This compound would potentially be able to be used as an MR imaging probe to detect vascular damage. We are now investigating the use of this compound in *ex vivo* and *in vivo* trials. These results will be reported in due course.

Acknowledgements

This work was supported by a Grant-in-Aid for Scientific Research from the Ministry of Education, Culture, Sports, Science, and Technology of Japan and also from the Ministry of Health, Labour, and Welfare of Japan.

References

1. R. Ross, *Nature*, **1993**, *362*, 801.
2. X. Yu, S. K. Song, J. Chen, M. J. Scott, R. J. Fuhrhop, C. S. Hall, P. J. Gaffney, S. A. Wickline, and G. M. Lanza, *Magn. Reson. Med.*, **2000**, *44*, 867.
3. H. Maaheimo, R. Renkonen, J. Turunen, L. Penttila, and O. Renkonen, *Eur. J. Biochem.*, **1995**, *234*, 616.
4. M. Lewin, N. Carlesso, C. H. Tung, X. W. Tang, D. Cory, D. T. Scadden, and R. Weissleder, *Nature Biotech.*, **2000**, *18*, 410.
5. H. R. Wabinga, *East Afr. Med. J.*, **1996**, *73*, S19.
6. J. R. Woods, Jr. and H. Maibach, *Obstet. Gynecol.*, **1979**, *53*, 602.
7. N. A. Dezutter, R. M. Sciot, T. J. de Groot, G. M. Bormans, and A. M. Verbruggen, *Nucl. Med. Commun.*, **2001**, *22*, 553.
8. B. C. Christensen, J. Chemnitz, and I. Tkocz, *Acta Pathol. Microbiol. Scand.: A*, **1976**, *84*, 355.
9. S. Citi, *J. Cell. Biol.*, **1993**, *121*, 485.